The Astrophysical Journal, 622:772–796, 2005 April 1

A REDSHIFT SURVEY OF THE SUBMILLIMETER GALAXY POPULATION

S. C. Chapman,[1] A. W. Blain,[1] Ian Smail,[2] and R. J. Ivison[3,4]

Received 2004 July 22; accepted 2004 December 13

ABSTRACT

We have obtained spectroscopic redshifts using the Keck I telescope for a sample of 73 submillimeter galaxies (SMGs), with a median 850 μm flux density of 5.7 mJy, for which precise positions are available through their faint radio emission. The galaxies lie at redshifts out to $z = 3.6$, with a median redshift of 2.2 and an interquartile range $z = 1.7$–2.8. Modeling a purely submillimeter flux–limited sample, based on the expected selection function for our radio-identified sample, suggests a median redshift of 2.3, with a redshift distribution remarkably similar to the optically and radio-selected quasars. The observed redshift distributions are similar for the active galactic nucleus (AGN) and starburst subsamples. The median $R_{\rm AB}$ is 24.6 for the sample. However, the *dust-corrected* ultraviolet (UV) luminosities of the galaxies rarely hint at the huge bolometric luminosities indicated by their radio/submillimeter emission, with the effect that the true luminosity can be underestimated by a median factor of $\sim$120 for SMGs with pure starburst spectra. Radio and submillimeter observations are thus essential to select the most luminous high-redshift galaxies. The 850 μm, radio, and redshift data are used to estimate the dust temperatures and characterize photometric redshifts. Using 450 μm measurements for a subset of our sample, we confirm that a median dust temperature of $T_d = 36 \pm 7$ K, derived on the assumption that the local far-infrared (FIR)–radio correlation applies at high redshift, is reasonable. Individual 450 μm detections are consistent with the local radio-FIR relation holding at $z \sim 2$. This median T_d is lower than that estimated for similarly luminous *IRAS* 60 μm galaxies locally. We demonstrate that dust temperature variations make it impossible to estimate redshifts for individual SGMs to better than $\Delta z \simeq 1$ using simple long-wavelength photometric methods. We calculate total infrared and bolometric luminosities (the median infrared luminosity estimated from the radio is $8.5^{+7.4}_{-4.6} \times 10^{12}\ L_{\odot}$), construct a luminosity function, and quantify the strong evolution of the submillimeter population across $z = 0.5$–3.5 relative to local *IRAS* galaxies. We use the bolometric luminosities and UV-spectral classifications to determine a lower limit to the AGN content of the population and measure directly the varying the contribution of highly obscured, luminous galaxies to the luminosity density history of the universe for the first time. We conclude that bright submillimeter galaxies contribute a comparable star formation density to Lyman break galaxies at $z = 2$–3, and including galaxies below our submillimeter flux limit, this population may be the dominant site of massive star formation at this epoch. The rapid evolution of SMGs and QSO populations contrasts with that seen in bolometrically lower luminosity galaxy samples selected in the rest-frame UV and suggests a close link between SMGs and the formation and evolution of the galactic halos that host QSOs.

Subject headings: cosmology: observations — galaxies: evolution — galaxies: formation — galaxies: starburst

1. INTRODUCTION

The submillimeter galaxy (SMG) population was first detected 7 years ago with the Submillimeter Common User Bolometer Array (SCUBA; Holland et al. 1999) on the James Clerk Maxwell Telescope (JCMT; Smail et al. 1997; Hughes et al. 1998; Barger et al. 1998; Eales et al. 1999). The discovery of SMGs motivated a variety of surveys using both SCUBA and a similar instrument, the Max-Planck Millimeter Bolometer (MAMBO; Bertoldi et al. 2000; Kreysa et al. 2002), on the IRAM 30 m telescope. Several surveys were undertaken of blank fields, using different strategies to determine their depths and area coverage (Barger et al. 1999a, 2002; Eales et al. 2000; Scott et al. 2002; Borys et al. 2003; Serjeant et al. 2003; Webb et al. 2003a; Dannerbauer et al. 2004; Greve et al. 2004). These surveys detect sources at a rate of approximately one source per night. A second class of survey used massive clusters to provide a mild gravitational lensing boost to aid in the detection and study of SMGs. These surveys uncovered sources at a rate of about two per night (for example, Smail et al. 2002; Chapman et al. 2002b; Cowie et al. 2002; and Knudsen 2004).

These surveys have gradually built up a large enough sample of SMGs to produce a statistically useful count (e.g., Blain et al. 2002). However, until very recently, most of our detailed knowledge of the properties of SMGs came from a handful of SMGs identified in lensing cluster fields (e.g., Ivison et al. 1998, 2000, 2001; Frayer et al. 1998, 1999, 2004), since performing follow-ups of blank field sources without the lensing boost required significantly more resources (e.g., Gear et al. 2000; Lutz et al. 2001; Dannerbauer et al. 2002; Dunlop et al. 2004).

A breakthrough in our understanding of the properties of SMGs came from exploiting ultradeep 20 cm radio maps. A strong correlation exists between the far-infrared (FIR) and radio flux densities of galaxies, both locally and at high redshifts (e.g., Helou et al. 1985; Condon 1992; Garrett 2002), and so deep radio imagery with the Very Large Array (VLA)[5] can be used to

[1] California Institute of Technology, 1200 East California Boulevard, Pasadena, CA 91125.
[2] Institute for Computational Cosmology, University of Durham, South Road, Durham DH1 3LE, UK.
[3] Astronomy Technology Centre, Royal Observatory, Blackford Hill, Edinburgh EH9 3HJ, UK.
[4] Institute for Astronomy, University of Edinburgh, Blackford Hill, Edinburgh EH9 3HJ, UK.

[5] The National Radio Astronomy Observatory is a facility of the National Science Foundation operated under cooperative agreement by Associated Universities, Inc.

help pinpoint and study SMGs (Ivison et al. 1998; Smail et al. 2000; Barger et al. 2000; Chapman et al. 2001a, 2002a). These radio maps provide a $\sim 1\farcs5$ beam and $\sim 0\farcs5$ astrometric precision relative to the optical frame, sufficient to accurately locate the counterpart of a submillimeter source. The use of radio imaging has culminated in the successful identification of at least 65% of SMGs brighter than $S_{850\,\mu\mathrm{m}} > 5$ mJy and their photometric characterization in the optical/near-infrared waveband (Ivison et al. 2002; Chapman et al. 2003c; Wang et al. 2004; Borys et al. 2004; Greve et al. 2004).

The ability to precisely locate the position of submillimeter emitting source is essential if we wish to study their properties in any detail. In particular, this is a necessary first step in efforts to derive redshifts and luminosities for these systems. It had been hoped that long-wavelength observations of the dust emission spectrum of these galaxies might be prove a reliable route to derive their redshifts and luminosities. The submillimeter/radio flux ratio was first used by Carilli & Yun (1999) in this manner to estimate the typical redshift of SMGs; however, the technique was recognized immediately to have limited accuracy ($\sim$50% redshift errors) whenever a range of dust temperatures (T_d) was present. This uncertainty is particularly important for deriving luminosities and related properties from submillimeter observations as the submillimeter flux density is $S_{850\,\mu\mathrm{m}} \propto T_d^{\simeq 3.5}$ for a fixed FIR luminosity at $z \simeq 2$. In addition, there is a strong degeneracy between T_d and $1 + z$ (Blain 1999), which limits the usefulness of simple photometric redshifts for estimating luminosities for the SMG population. Refinement of the modeling and fitting techniques appears not to have overcome this basic source of uncertainty (e.g., Aretxaga et al. 2003; Wiklind 2003). Indeed, even surveys at several submillimeter wavelengths (e.g., Hughes et al. 2002) cannot completely overcome the degeneracy between dust temperature and redshift (Blain 1999; Blain et al. 2003; see also Aretxaga et al. 2004 for a contrary view).

As a consequence, precise redshifts are crucial for interpreting almost every aspect of SMGs. Prior to 2002, only a handful of spectroscopic redshifts were available for unambiguously identified SMGs (Ivison et al. 1998, 2000; Barger et al. 1999b; Lilly et al. 1999). Recent attempts to measure redshifts for SMGs have met with more success (Chapman et al. 2002c, 2003c; Barger et al. 2002; Ledlow et al. 2002; Smail et al. 2003a, 2003b; Kneib et al. 2004). However, the resulting sample is still restricted in size and unrepresentative of the general properties of the SMG population (with a bias toward optically bright counterparts and a preponderance of strong-lined AGNs). A redshift survey of a large and representative sample of SMGs is therefore urgently required.

Chapman et al. (2003a, hereafter C03) demonstrated that spectroscopic redshifts can be obtained for even the optically faintest SMGs, spanning a factor of 100 in *I*-band flux, allowing a much more representative sample of the population to be studied. Their approach involved constructing densely packed distributions of SMGs across $\sim 10'$ fields (matched to the area coverage of multiobject spectrographs on 10 m telescopes) with precise positions from radio counterparts. These samples could then be efficiently and effectively targeted using deep spectroscopy in the UV/blue spectral region. With a large, unbiased sample of SMGs constructed in this manner, it is possible to address questions about the SMG population with more certainty, including their dust temperatures (T_d) and SED properties, their luminosities at various wavelengths and luminosity evolution, their contribution to the FIR background, and their relation to other populations of galaxies and AGNs at high redshift.

In this paper, we present an expanded sample from the 10 SMGs with robust spectroscopic redshifts described by C03 to provide a total sample of 73 redshifts for unambiguously identified SMGs. We discuss the properties and observations of this sample, along with selection effects, in § 2. We present the basic observational results obtained for this sample, including the redshift distributions, variation in SEDs with redshift as characterized by the submillimeter/radio flux ratio, and optical properties in § 3. In § 4 we then use basic assumptions to derive dust temperatures and bolometric luminosities for our sample, compare the UV properties of the galaxies with their radio/submillimeter emission, assess their contribution to the luminosity and star formation histories of the universe and the FIR background (FIRB), and discuss their evolutionary connections with other high-redshift populations. Finally, in § 5 we give our main conclusions. All calculations assume a flat, ΛCDM cosmology with $\Omega_\Lambda = 0.7$ and $H_0 = 71$ km s^{-1} Mpc^{-1}.

2. SAMPLE DEFINITION, OBSERVATIONS, AND ANALYSIS

The parent sample of SMGs used for our survey consists of 150 sources detected at 850 μm (>3 σ) with SCUBA/JCMT, in seven separate fields (the field centers are listed in Table 1): CFRS03, Lockman Hole, Hubble Deep Field (HDF), SSSA13, Westphal-14, ELAIS-N2, and SSSA22. Of these SMGs, 104 have radio identifications from deep VLA radio maps at 1.4 GHz. This radio-identified subset is the focus of this paper.

In all fields the SCUBA submillimeter data were retrieved from the JCMT archive[6] and reduced in a consistent manner using the SURF reduction tools (Jenness et al. 1998) and our own software to extract beam-weighted submillimeter fluxes.[7] In some cases, additional radio sources were targeted in SCUBA's *photometry* mode (Holland et al. 1999) to efficiently construct large samples of SMGs to target in contiguous regions around fields mapped by SCUBA (e.g., Chapman et al. 2001a, 2002a, 2003c). In addition, follow-up SCUBA photometry was used to verify the reality and submillimeter flux densities of 11 of the sources detected in SCUBA maps. These new SCUBA observations were obtained during JCMT observing runs in 2002 and 2003, with sky opacity at 225 GHz and $\tau_{225} = 0.04$–0.09. The observing strategy was to integrate for a fixed length of time (1.0 hr) on all targeted galaxies, with additional time allocated to targets that did not achieve our nominal rms sensitivity goal of $dS_{850} = 1.5$ mJy because of weather conditions. We note the observational mode used to identify sources in Table 2, based on whether their submillimeter detection was obtained entirely in *photometry* mode (P), entirely in mapping mode (M), or through a combination of the two modes (MP).

Radio data for these fields either existed from previous work by members of our group (Lockman Hole, ELAIS-N2) were rereduced for the purpose of this study (CFRS-03, SSSA22, Westphal-14) or were obtained from the public release (HDF; Richards 2000). The SSSA13 radio data were obtained from E. A. Richards (2004, private communication) and are so far unpublished (a subsequent reduction of the SSSA13 data is described in E. Fomalont et al. 2005, in preparation). The radio

[6] The JCMT is operated by the Joint Astronomy Centre on behalf of the UK Particle Physics and Astronomy Research Council, the Netherlands Organization for Scientific Research, and the National Research Council of Canada. The JCMT archive is provided through the Canadian Data Archive Center.

[7] Map fluxes are obtained by extracting the effective beam imprint $(-0.5, 1, -0.5)\delta$ SCUBA chopping/nodding profile (e.g., Scott et al. 2002; Borys et al. 2003).

TABLE 1
FIELD PROPERTIES

NAME	RADIO CENTER (J2000) R.A.	RADIO CENTER (J2000) Decl.	RADIO DEPTH[a] (μJy)	N_{SMG} MAP[b]	N_{SMG} PHOT.[b]	$N_{spectra}$[c]	$N_{redshifts}$[d]	OPTICAL DATA COMMENTS[e]
CFRS-03	03 02 40.9	00 09 08	10	9	0	9	6	CFH12K, LRIS
Lockman.....	10 52 00.1	57 18 10	5	10	0	8	4	MOSAIC, CFH12K, Suprime
HDF-N	12 37 07.2	62 14 02	8	27	11	31	24	MOSAIC, Suprime
SSA-13.....	13 12 16.5	42 41 21	4	9	8	16	9	MOSAIC, Suprime
CFRS-14	14 17 49.4	52 30 23	14	8	1	9	8	Cosmic, WHT, CFH12k
ELAIS-N2	16 36 50.0	40 57 35	15	8	3	10	10	WHT, LFC
SSA-22.....	22 15 15.1	00 13 55	8	7	8	15	11	CFH12K, LFC, cosmic

NOTE.—Units of right ascension are hours, minutes, and seconds, and units of declination are degrees, arcminutes, and arcseconds.
[a] The 1 σ radio depth at phase center.
[b] Number of radio-identified submillimeter sources above 3 σ divided into SCUBA mapping and SCUBA photometry observations. Photometry observations targeted the radio source position.
[c] Number of spectra attempted.
[d] Number of successful redshifts.
[e] Optical data used in the identifications: CFHT/CFH12K (Cuillandre et al. 2000), KPNO 4 m/MOSAIC (Muller et al. 1998), Subaru/Suprime (Komiyama et al. 2003), WHT/PFC (Tulloch 2000), Palomar 200 inch-LFC/cosmic (Simcoe et al. 2000).

data for the Lockman Hole and ELAIS-N2 fields come from Ivison et al. (2002), who identified counterparts to the SMGs in these regions from Scott et al. (2002). For those fields that we rereduced, the radio data were retrieved from the VLA archive, when available, and combined with new data obtained by our group in SSSA22 (36 hr; A configuration), Westphal-14 (24 hr; B configuration), and CFRS-03 (16 hr; B configuration). The radio maps were reduced in an identical manner to those described in Ivison et al. (2002). The resulting radio maps have depths range from 4 to 10 μJy rms (see Table 1).

Deep optical imaging in the *B*, *R*, and *I* passbands is available for all of our fields. This consists of several-hour integrations with mosaic CCD cameras on 4 and 8 m class telescopes, taken either from public archives, or obtained by our group during observing runs throughout 2000–2002. HDF (*BRI*), SSA13 (*I*), and Lockman (*RI*) imaging was obtained with the Suprime camera on the Subaru Telescope. The HDF data were retrieved from the public release presented in Capak et al. (2004). The SSA13 and Lockman data were retrieved from the Subaru archive and reduced by our group. The *BR* imaging in SSA13 was obtained with the Kitt Peak 4 m telescope and the MOSAIC camera and reduced with the *mscred* tasks in IRAF. The *B* imaging in Lockman and the ELAIS-N2 imaging (*BRI*) were obtained with the wide-field camera on the William Herschel Telescope (WHT) and reduced in a standard manner using IRAF. The *g*, *Rs*, and *I* imaging in SSA22 and Westphal-14 was obtained from the public release in Steidel et al. (2003), and the details are described therein. Additional SSA22 imaging was obtained with the Large Format Camera (LFC) instrument (*g*) on the Palomar 200 inch (5 m) telescope and the Canada-France-Hawaii Telescope (CFHT) 12k mosaic camera (*R* and *I*) and was reduced with *mscred* in IRAF. References to all these instruments are listed in Table 1. Near-infrared imaging is also available for the majority of submillimeter sources in our fields from a number of different instruments and telescopes, typically reaching at least $K = 20$ and $J = 22$. Details of the optical, radio, and submillimeter data in each field are given in Table 1. The near-IR properties of our SMGs are discussed fully in Smail et al. (2004).

SMGs with radio identifications allow the position of the rest-frame FIR emission to be unambiguously identified with a position in the optical imaging to within the relative astrometric alignment of the radio/optical frames. Optical images were distortion-corrected and tied to the same astrometric grid as the radio data using large numbers of optically bright radio sources across the field, resulting in an rms positional uncertainty of typically $\sim 0\farcs5$ (see the detailed discussions in Richards [2000] and Ivison et al. [2002]). The R_{AB} magnitudes (subsequently termed *R*) in $2''$ apertures of the targets range from $R = 18.3$ to $R > 27.5$ (Fig. 1).

Targets were selected for spectroscopic follow-up from the seven fields, chosen at random and prioritized equally, *without preference for optical brightness*. Observations of two sources were obtained with Echellette Spectrograph and Imager (ESI) on the Keck II telescope[8] on the night of 2001 July 16 and have been previously discussed by Chapman et al. (2002c). Over the course of seven observing runs between 2002 March and 2004 February we observed 98 of the 104 sources in our radio SMG sample with the Low Resolution Imaging Spectrograph (LRIS; Oke et al. 1995) spectrograph on the Keck I telescope obtaining reliable redshifts for a total of 73 galaxies. The first 10 spectroscopic identifications from our program were presented in C03.

The details of the spectroscopic configurations for our observing runs and their success rates are presented in Table 3. Observations were taken with LRIS using several different settings of gratings and cameras. Data taken before 2002 March were obtained before the commissioning of the large mosaic CCD blue camera and used a smaller format blue device. All subsequent data was taken with the larger format ($4k \times 4k$) blue camera (Steidel et al. 2004). Our observations use either the 5600 Å (D560) or 6800 Å (D680) dichroic to divide the light between the red and blue cameras. The 400 line mm^{-1} (B400) grism was always used in the blue arm to provide wavelength coverage from the atmospheric limit out to the dichroic wavelength for most of the slitlets on the masks. This grism provides reasonable resolution ($\sim$5–6 Å) with our adopted $1\farcs2$–$1\farcs4$ slit widths. Either the 400 line mm^{-1} (R400) or 600 line mm^{-1} (R600) gratings were used in the red arm, depending on the

[8] The data presented herein were obtained at Some of the data presented herein were obtained at the W. M. Keck Observatory, which is operated as a scientific partnership among the California Institute of Technology, the University of California, and the National Aeronautics and Space Administration. The Observatory was made possible by the generous financial support of the W. M. Keck Foundation.

TABLE 2

PROPERTIES OF RADIO SMGS

ID	$S_{1.4\ \mathrm{GHz}}$[a] (μJy)	B_{AB} (mag)	R_{AB} (mag)	$S_{850\ \mu\mathrm{m}}$ (mJy)	z	$L_{\mathrm{bol}} \times 10^{12}$ ($L_{\odot}$)	T_d (K)	Comment
SMM J030226.17+000624.5	481.5 ± 9	19.1	17.8	7.9 ± 1.6	0.080	0.03	11.4	M; probable lens
SMM J030227.73+000653.5	217 ± 9	23.8	22.9	4.4 ± 1.3	1.408	27.8	56.4	M; Lyα, abs, Hα (SB)
SMM J030231.81+001031.3	45.1 ± 9	>26.4	>25.1	5.0 ± 1.5	1.316	1.3	25.6	M; O II (SB)
SMM J030236.15+000817.1	42.1 ± 9.1	>26.4	26.1	3.4 ± 0.6	2.435	6.7	41.3	M; Fe II, Hα, N II (SB)
SMM J030238.62+001106.3	347.3 ± 9	25.6	24.3	4.1 ± 1.4	0.276	0.21	25.5	M; O II, Ne V (AGN)
SMM J030244.82+000632.3	154.0 ± 34.1	20.5	19.1	4.9 ± 1.1	0.176	0.12	13.5	M; O II, Hα (SB)
SMM J105151.69+572636.0	134.4 ± 13.0	n/a	25.2	6.7 ± 1.7	1.147	1.6	25.4	M; O II, Mg II (SB)
SMM J105155.47+572312.7[b]	46.3 ± 10.2	23.8	23.2	5.7 ± 1.4	2.686	11.7	41.7	M; Lyα, IS abs, Hα (SB)
SMM J105158.02+571800.2	98.1 ± 11.6	n/a	24.1	7.7 ± 1.7	2.239	12.3	39.2	M; Lyα abs, C IV abs, Hα (SB)
SMM J105200.22+572420.2[c]	57.4 ± 13.2	n/a	22.1	5.1 ± 1.3	0.689	0.33	20.0	M; O II, Fe II (SB)
SMM J105201.25+572445.7	72.1 ± 10.2	n/a	25.7	9.9 ± 2.2	2.148	8.1	33.0	M; Lyα abs, Hα (SB)
SMM J105207.49+571904.0	277.8 ± 11.9	n/a	26.0	6.2 ± 1.6	2.689	17.5	45.4	M; Lyα, Hα (SB)
SMM J105225.79+571906.4[d]	127.4 ± 5.1	n/a	24.7	4.9 ± 1.5	2.372	18.7	49.3	M; Lyα, IS abs (SB)
SMM J105227.77+572218.2[b]	40.4 ± 9.4	n/a	26.0	7.0 ± 2.1	1.956	3.5	23.9	M; Lyα, C IV (SB)
SMM J105227.58+572512.4	39.2 ± 11.4	n/a	25.0	4.5 ± 1.3	2.142	4.0	33.7	M; IS abs, C III (SB)
SMM J105230.73+572209.5	86.3 ± 15.4	n/a	23.3	11 ± 2.6	2.611	14.5	37.1	M; Lyα, Si II, Hα (SB)
SMM J105238.19+571651.1[d]	71.1 ± 12.6	n/a	22.7	5.3 ± 1.6	1.852	5.8	35.9	M; IS abs (SB)
SMM J105238.30+572435.8[b]	61.0 ± 22.0	n/a	24.6	10.9 ± 2.4	3.036	18.1	39.4	M; Lyα, C IV (AGN)
SMM J123549.44+621536.8	74.6 ± 9.5	24.2	23.7	8.3 ± 2.5	2.203	8.9	35.4	P; IS abs, Hα, CO (3–2) (SB)
SMM J123553.26+621337.7[b]	58.4 ± 9.0	24.8	24.7	8.8 ± 2.1	2.098	6.1	31.6	P; IS abs (SB)
SMM J123555.14+620901.7	212.0 ± 13.7	24.5	24.2	5.4 ± 1.9	1.875	16.2	46.8	P; Lyα, IS abs (SB)
SMM J123600.10+620253.5	262.0 ± 17.1	25.7	25.4	6.9 ± 2.0	2.710	56.2	59.9	P; extended Lyα (SB)
SMM J123600.15+621047.2	131.0 ± 10.6	25.4	25.1	7.9 ± 2.4	1.994	12.0	39.0	P; Lyα, Hα (SB)
SMM J123606.72+621550.7	24.0 ± 5.9	23.5	23.6	4.4 ± 1.4	2.416	3.7	33.1	M; Lyα, Si IV, C IV (AGN)
SMM J123606.85+621021.4	74.4 ± 4.1	25.6	25.2	11.6 ± 3.5	2.509	12.8	35.5	P; Lyα, Hα (SB)
SMM J123616.15+621513.7[e]	53.9 ± 8.4	26.8	25.7	5.8 ± 1.1	2.578	10.0	39.9	M; Lyα (SB)
SMM J123618.33+621550.5[b]	151.0 ± 11.0	26.0	25.9	7.3 ± 1.1	1.865	11.4	39.4	M; IS abs (SB)
SMM J123621.27+621708.4[e]	148.0 ± 11.0	25.1	24.9	7.8 ± 1.9	1.988	13.5	40.3	M; IS abs, Hα (SB)
SMM J123622.65+621629.7	70.9 ± 8.7	25.6	25.4	7.7 ± 1.3	2.466	11.6	38.6	M; Lyα, Hα (SB)
SMM J123629.13+621045.8	81.4 ± 8.7	26.1	24.6	5.0 ± 1.3	1.013	1.2	26.0	M; O II, Mg II (SB)
SMM J123632.61+620800.1	90.6 ± 9.3	23.8	23.6	5.5 ± 1.3	1.993	8.2	40.0	M; Lyα, N V, Si IV, C IV (AGN)
SMM J123634.51+621241.0	230.0 ± 13.8	24.4	23.9	4.3 ± 1.4	1.219	5.5	37.5	M; O II, Mg II (SB)
SMM J123635.59+621424.1	87.8 ± 8.8	24.2	24.2	5.5 ± 1.4	2.005	8.1	40.3	M; Lyα, C IV (AGN)
SMM J123636.75+621156.1	39.0 ± 8.0	21.9	21.6	7.0 ± 2.1	0.557	0.12	15.2	M; O II, Ne V (AGN)
SMM J123651.76+621221.3[b]	49.3 ± 7.9	21.6	21.4	4.6 ± 0.8	0.298	0.08	13.3	M; probable lens
SMM J123707.21+621408.1[c]	45.0 ± 7.9	26.9	26.0	4.7 ± 1.5	2.484	7.5	39.2	M; Lyα, Hα (SB)
SMM J123711.98+621325.7[c]	53.9 ± 8.1	26.0	25.8	4.2 ± 1.4	1.992	4.9	36.3	M; Lyα, Hα (SB)
SMM J123712.05+621212.3	21.0 ± 4.0	27.0	25.5	8.0 ± 1.8	2.914	5.5	31.3	M; Lyα, C IV (AGN)
SMM J123716.01+620323.3	109.0 ± 11.4	20.3	20.2	5.3 ± 1.7	2.037	10.5	41.7	P; Lyα, N V, Si IV, C IV (QSO)
SMM J123721.87+621035.3	41.0 ± 9.0	24.3	23.3	12.0 ± 3.9	0.979	0.53	16.9	M; Hα, Fe II, (AGN)
SMM J131201.17+424208.1	49.1 ± 6.0	25.2	24.0	6.2 ± 1.2	3.405	20.2	47.1	MP; Lyα, Si IV, C IV, O III, CO (4–3) (AGN)
SMM J131208.82+424129.1	82.4 ± 4.8	25.7	23.9	4.9 ± 1.5	1.544	3.7	33.2	M; Hα, Mg II, C IV (AGN)
SMM J131212.69+424422.5	102.6 ± 7.4	>27	26.7	5.6 ± 1.9	2.805	24.3	50.7	M; Lyα, Si IV, C IV (AGN)

TABLE 2—*Continued*

ID	$S_{1.4\ \mathrm{GHz}}$[a] (μJy)	B_{AB} (mag)	R_{AB} (mag)	$S_{850\ \mu\mathrm{m}}$ (mJy)	z	$L_{\mathrm{bol}} \times 10^{12}$ ($L_{\odot}$)	T_d (K)	Comment
SMM J131215.27+423900.9	69.3 ± 4.0	18.6	18.3	4.4 ± 1.0	2.565	12.7	45.7	MP; Lyα, C IV, He II (QSO)
SMM J131222.35+423814.1	26.3 ± 3.9	21.8	20.2	3.0 ± 0.9	2.565	4.8	39.2	MP; Lyα, C IV, He II (AGN)
SMM J131225.20+424344.5	76.4 ± 6.8	23.3	22.1	2.4 ± 0.8	1.038	1.2	31.4	M; O II, Fe II (SB)
SMM J131228.30+424454.8	50.9 ± 8.1	25.9	24.7	3.4 ± 0.9	2.931	13.6	49.7	M; Lyα, C IV (SB)
SMM J131231.07+424609.0	39.4 ± 8.5	>27	26.9	4.9 ± 1.6	2.713	8.5	39.9	MP; Lyα (SB)
SMM J131225.73+423941.4	752.5 ± 4.2	24.4	24.2	4.1 ± 1.3	1.554	33.8	62.2	MP; Mg II, Fe II, C IV, Si II (SB)
SMM J131232.31+423949.5	94.8 ± 4.3	25.7	24.6	4.7 ± 1.1	2.320	13.1	45.4	M; Lyα, Hα (SB)
SMM J131239.14+424155.7	49.8 ± 6.6	26.0	25.7	7.4 ± 1.9	2.242	6.3	33.2	M; Lyα, Hα (SB)
SMM J141742.04+523025.7	232 ± 23	19.7	19.4	2.6 ± 0.9	0.661	1.2	33.7	M; O II, Mg II (SB)
SMM J141741.81+522823.0	80 ± 16	23.0	21.5	3.3 ± 1.0	1.150	1.7	31.1	M; O II, Fe II (SB)
SMM J141800.40+512820.3	128 ± 19	24.1	23.3	5.0 ± 1.0	1.913	11.1	43.2	M; Lyα, IS abs (SB)
SMM J141809.00+522803.8[b]	67 ± 15	25.8	25.7	4.3 ± 1.0	2.712	14.4	47.4	M; Lyα (SB)
SMM J141802.87+523011.1	39 ± 14	24.4	24.2	3.4 ± 0.9	2.127	4.9	38.3	M; IS abs (SB)
SMM J141750.50+523101.0	57 ± 14	25.1	25.0	2.8 ± 0.9	2.128	5.8	42.1	M; Lyα, IS abs (SB)
SMM J141813.54+522923.4	93.0 ± 16.0	27.4	25.9	3.6 ± 1.1	3.484	39.1	68.5	MP; Lyα, C IV (AGN)
SMM J163627.94+405811.2	92 ± 23	25.2	24.9	6.5 ± 2.1	3.180	31.1	52.1	M; Lyα, O I, C IV, Hα (AGN)
SMM J163631.47+405546.9[b]	99 ± 23	24.9	24.1	6.3 ± 1.9	2.283	13.1	42.0	M; Lyα, C IV (AGN)
SMM J163639.01+405635.9	159 ± 27	24.6	23.8	5.1 ± 1.4	1.495	6.4	32.7	M; C IV, He II, C III, Fe II, Hα (SB)
SMM J163650.43+405734.5[c]	221 ± 16	23.3	22.5	8.2 ± 1.7	2.378	32.8	49.9	M; Lyα, IS abs, C IV, Hα, CO (3–2) (AGN/SB)
SMM J163658.19+410523.8	92 ± 16	26.0	25.8	10.7 ± 2.0	2.454	14.9	37.7	M; Lyα, Hα, CO (3–2) (SB)
SMM J163658.78+405728.1[b]	74 ± 29	23.9	22.7	5.1 ± 1.4	1.190	1.7	27.5	M; O II, Mg II (SB)
SMM J163704.34+410530.3	45 ± 16	24.2	23.1	11.2 ± 1.6	0.840	0.40	16.5	M; O II, O III (SB)
SMM J163706.51+405313.8	74 ± 23	n/a	24.6	11.2 ± 2.9	2.374	10.9	34.3	P; Lyα, Si IV, C IV, Hα (AGN)
SMM J221724.69+001242.1[b]	121.1 ± 10.7	20.4	20.0	8.6 ± 1.9	0.51	0.25	15.9	M; probable lens
SMM J221733.12+001120.2	69.2 ± 10.3	22.8	21.4	6.9 ± 2.1	0.652	0.33	18.8	MP; O II, Mg II, Fe II (SB)
SMM J221804.42+002154.4[b]	43.8 ± 10.4	25.2	24.7	9.0 ± 2.3	2.517	7.6	33.1	P; IS abs (SB)
SMM J221806.77+001245.7	241.5 ± 11.2	25.8	24.3	8.4 ± 2.3	3.623	118.6	72.0	P; Lyα, O III (SB)
SMM J221735.84+001558.9	44.3 ± 12.8	26.6	25.5	4.9 ± 1.3	3.089	13.1	44.6	M; Lyα (SB)
SMM J221735.15+001537.2	49.4 ± 13.3	26.1	25.7	6.3 ± 1.3	3.098	15.3	43.6	M; Lyα, CO (3–2) (SB)
SMM J221733.91+001352.1	44.5 ± 13.4	24.8	24.1	9.1 ± 1.1	2.555	8.1	33.6	M; IS abs, Hα (SB)
SMM J221725.97+001238.9	41.2 ± 9.3	>27	27.1	17.4 ± 2.9	3.094	12.9	32.1	Lyα, IS abs, CO (4–3) (SB)
SMM J221733.02+000906.0	161.7 ± 16.3	24.5	23.8	11.1 ± 3.4	0.926	1.9	26.4	MP; Fe II, Hα (SB)
SMM J221737.39+001025.1	110.1 ± 14.0	25.1	24.6	6.1 ± 2.0	2.614	21.4	44.0	MP; Lyα, IS abs (SB)

[a] The radio flux error estimates are based on the integrated radio flux and do not always reflect the point source detection sensitivity in the radio map.

[b] These SMGs have double radio source identifications, both confirmed to lie at the same redshift.

[c] These SMGs have double radio source identifications, one lying at the tabulated redshift and a second lying at $z < 0.5$. In calculations and figures presented herein, we have inferred based on the radio luminosity that the high-redshift source is the dominant contributor to the submillimeter emission.

[d] These SMGs have double radio source identifications; however, only one has a spectroscopic redshift.

[e] These SMGs have spectroscopically identified optical sources which are offset from the radio source identifications (typically $\sim 1''$), although it is usually the case that the optical identification is extended and overlaps the radio source. Chapman et al. (2004) addresses these issues through higher spatial resolution radio and optical imagery.

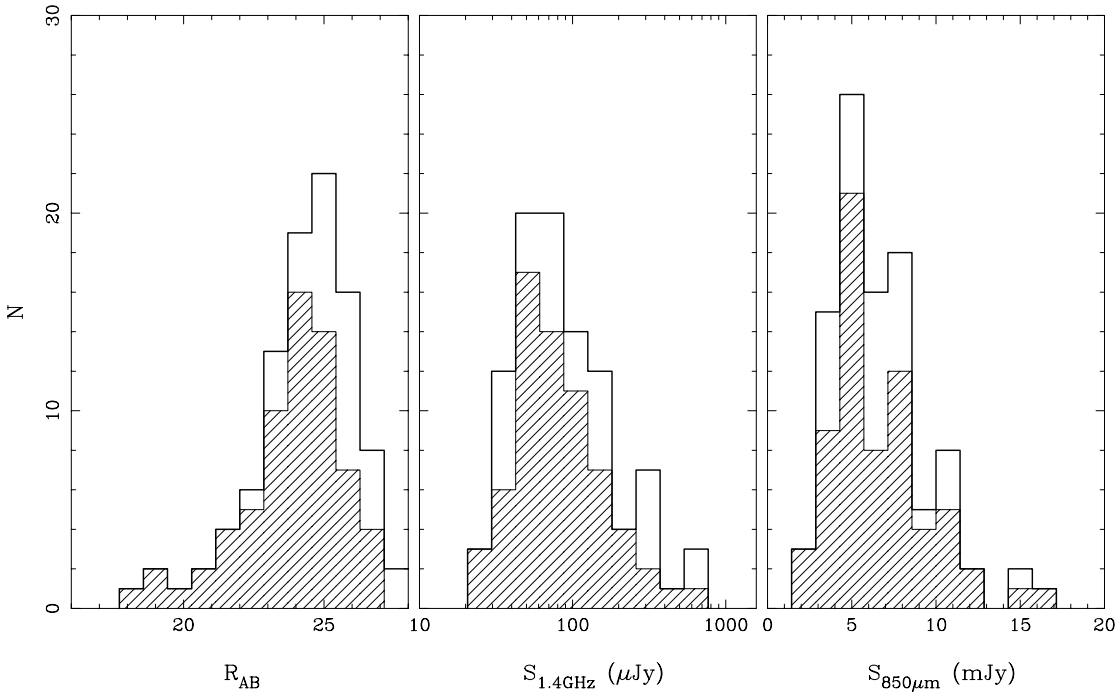

FIG. 1.—Comparison of our spectroscopically identified sample with the parent catalog of all SMGs identified in the radio waveband and observed spectroscopically. We show the relative distributions of *R*-magnitude, radio flux, and submillimeter flux (*shaded histograms are the spectroscopic sample*). As expected, the spectroscopically unidentified galaxies are typically fainter in the optical but have similar 1.4 GHz/850 μm ratios, consistent with the suggestion that they are likely to lie at similar redshifts to our spectroscopically identified sample but are on average more obscured in their rest-frame UV.

dichroic selected. Spectral resolutions of ~6–8 Å are achieved in the red.

Integration times were between 1.5–6.0 hr in dark or gray conditions, split into 30 minute exposures. Conditions varied from photometric to light cirrus, and seeing ranged between 0.″7 and 1.″1. Data reduction followed standard multislit techniques using custom IRAF scripts. The spectra typically probe an observed wavelength range of 3100–8000 Å.

2.1. *Spectroscopic Identifications*

To obtain redshifts from our spectroscopic observations, one-dimensional spectra were compared with template spectra and emission-line catalogs. Of the 98 radio SMGs observed, redshifts were obtained with confidence for 73 galaxies, for a total spectroscopic completeness of ~75%. The distribution of the optical, radio, and submillimeter fluxes of the parent and spectroscopically identified sample are shown in Figure 1. Representative spectra are shown in Figure 2. Table 1 lists the number of radio SMGs observed with LRIS in each field and the number of successful redshift measurements. Field-to-field variations reflect weather quality, as well as intrinsic source properties (e.g., Lyα line strength).

Twelve SMGs from our sample have previously published redshifts from other groups: SMM J141741.90+522823.6 and SMM J141742.20+523026.0 by Eales et al. (2000); SMM J030244.56+000632.3 by Webb et al. (2003); and SMM J123629.13+621045.8, J123632.61+620800.1, J123634.51+621241.0, J123635.59+621424.1, J123607.53+621550.4, J123721.87+621035.3, J131201.17+424208.1, J131215.27+423900.9, and J131225.20+424344.5 by Barger et al. (2001a, 2001b, 2003).[9] The R_{AB} magnitudes of these sources are among

[9] Note that not all these sources were measured as SMGs but were listed with spectroscopic redshifts in catalogs of radio or X-ray sources.

TABLE 3
OBSERVATION LOGS

Date	Field R.A.	Nights Clear	Configurations
	ESI		
2001 Jul 16	ELAIS-N2/SSA22	1	Echelle
	LRIS		
2002 Mar 18–21	Lockman/HDF/SSA13/ELAIS-N2	2	B400/D560/R600
2002 Sep 30–Oct 1	SSA22/CFRS03	2	B400/mirror
2002 Dec 26–27	CFRS03/Lockman/HDF	1	B400/D560/R600
2003 Mar 28–29	Lockman/HDF/Westphal-14	0.5	B400/D680/R400
2003 May 22–24	Lockman/HDF/Westphal-14/ELAIS-N2	2	B400/D560/R600
2003 Aug 22–23	ELAIS-N2/SSA22	2	B400/D560/R600
2004 Feb 14–15	Lockman/HDF/SSA13	2	B400/D560/R600

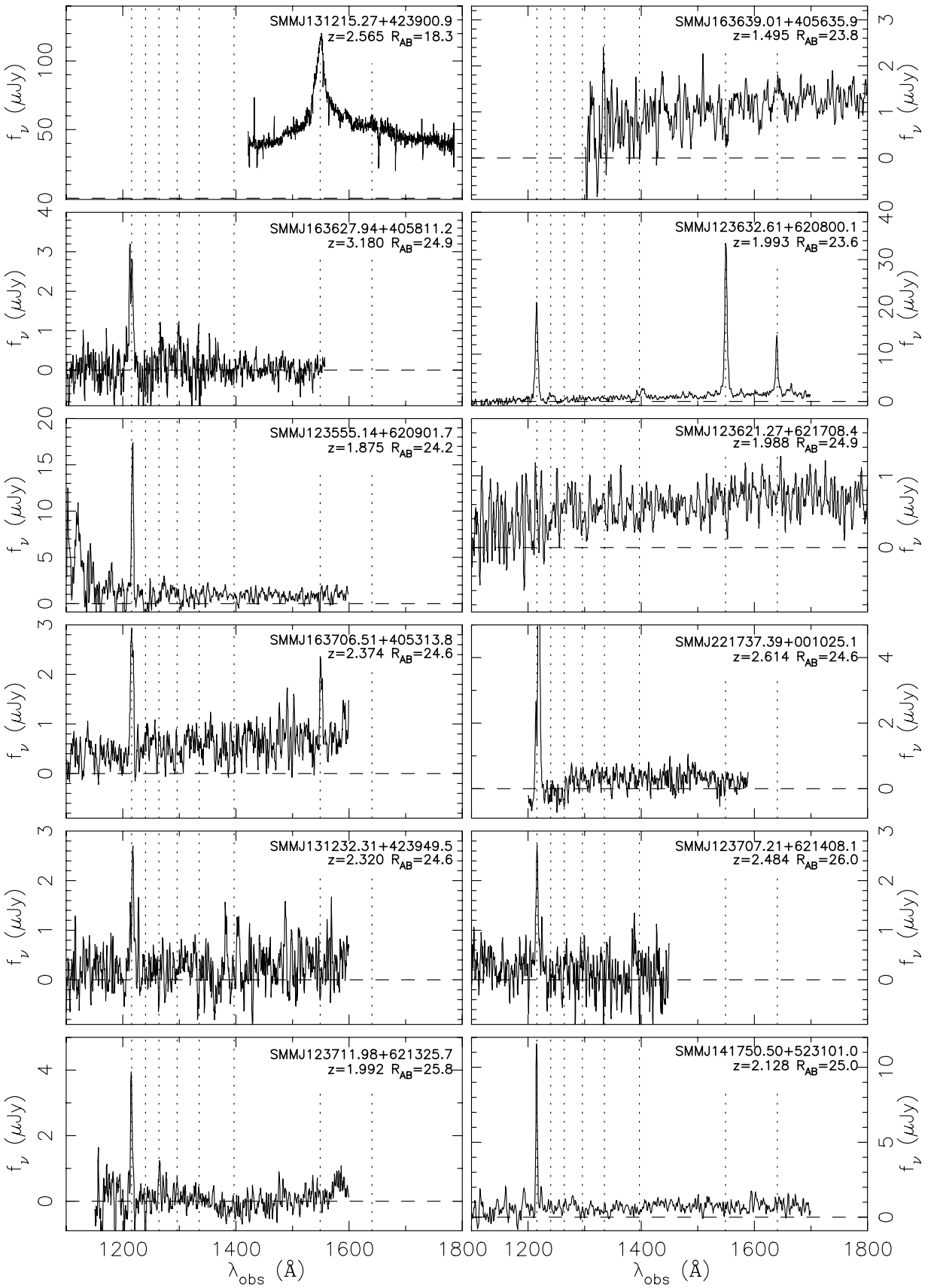

FIG. 2.—Representative spectra for 12 SMGs from our complete sample. The strongest UV lines used in the redshift identifications are marked by dashed lines. All spectra have been shifted to a common rest-frame wavelength scale.

the brightest in our sample, with an average of $R = 22.3 \pm 2.2$. All these redshifts from the literature are in agreement with our measurements within errors.

Three further sources were tentatively identified by Simpson et al. (2004) using the Subaru OH-airglow Suppressor. SMM J163658.19+410523.8 agrees with our redshift, as noted in Simpson et al. (2004). However, SMM J105158.02+571800.3 and SMM J141809.00+522803.8 disagree with our measured redshifts by $dz = 0.20$ and 0.16, respectively. Our redshift for SMM J105158.02+571800.3 ($z = 2.239$) is derived from two UV-absorption features and the detection of Hα (Swinbank et al. 2004), and we regard our redshift as a more robust identification. Our redshift for SMM J141809.00+522803.8 is derived primarily from strong Lyα in emission but lies at a redshift of $z = 2.71$, which makes it difficult to follow-up in nebular lines using near-IR spectrographs, casting some doubt on the reality of the Simpson et al. redshift. (Simpson et al. 2004 in fact suggest that their redshift is likely to be spurious on the basis of the weakness of the features and the residuals present from sky-line subtraction.)

The primary criteria for considering a redshift as robust is the identification of multiple emission/absorption lines. Our redshift identifications are confirmed by the detection of other lines and continuum features in 75% (55) of the identified spectra: AGN lines (C IV λ1549, S IV λ1397, N V λ1240), as well as weaker stellar and interstellar features and continuum breaks. We also consider redshifts to be robust if we detected a large equivalent width line (>20 Å) and there is supporting evidence that this line is Lyα. Only one-quarter (18) of the 73 spectroscopic redshifts are single-line identifications. There are three items of supporting evidence that are used to support the single-line Lyα identifications: the identification of a continuum break (if the continuum is detected) across the proposed Lyα line from the red to the blue (3/18), the absence of emission lines that do not match the proposed Lyα-derived redshift (all 18), and an asymmetrical line profile, with the blue wing truncated, which is typical of Lyα emission from high-redshift galaxies (8/18). In very few cases were identifications ambiguous using these criteria.

While single-line Lyα identifications may not be convincing to some readers, several arguments support our interpretation. For many of the single emission-line detections, the observed wavelength lies below 4000 Å (sometimes below 3700 Å), precluding a reasonable identification as [O II] λ3727 at $z < 0.07$ given the optical faintness and submillimeter/radio detection.

We also have two independent tests of the reliability of our redshifts. First, we have obtained Keck/NIRSPEC and VLT/ISAAC near-IR spectroscopic observations for a significant fraction of our sample to probe the nebular line emission to measure the star formation rates (SFRs), estimate metallicities, and study kinematics. These observations have successfully detected rest-frame Hα (and frequently [N II]) emission in 26 cases (Swinbank et al. 2004), confirming the UV-based redshifts in the present paper. Ten of the 18 single-line identifications have been confirmed in Hα. The near-IR Hα spectra were also able to break degeneracies in five cases in which spectral identifications based only on UV-absorption lines were consistent with two similar redshifts. These Hα/[N II] results were also used to aid in the spectroscopic classification of our sample, as indicated in Table 2.

Second, 15 of our SMG redshifts have been confirmed with CO line emission using the IRAM Plateau de Bure Interferometer (Neri et al. 2003; Greve et al. 2005), including two single-line identifications. These detections not only confirm the precision of the UV-based redshifts for the counterparts we targeted, but, equally importantly, they also confirm that these galaxies are gas-rich systems suitable to be the source of the luminous far-infrared emission detected in the submillimeter waveband.

The strength of the Lyα lines for the SMGs varies tremendously in both line flux (L_ν from 1 to 60 μJy) and rest-frame equivalent width, which ranges from -3 Å (absorption) to >150 Å (we note that we see no obvious variation in the radio/submillimeter properties of SMGs as a function of Lyα line strength). With the generally faint rest-frame UV continua exhibited by our SMG (65% are fainter than $R_{\rm AB} > 24.4$), there is a bias in our sample against obtaining redshifts for the weaker emission-line sources at the faintest continuum fluxes. This is reflected in Figure 1, in which the increased failure rate for obtaining spectroscopic redshifts is apparent for $R_{\rm AB} \gtrsim 24$. This bias is highlighted by the fact that sources with identifiable Lyα absorption only appear in our sample for SMGs with $R_{\rm AB} \lesssim 25$. We discuss the spectral properties and incompleteness of our sample in more detail in § 3.4.

3. RESULTS

3.1. *Sample Properties and Submillimeter/Radio Selection Effects*

To understand the characteristics of the submillimeter population we first have to quantify how the selection criteria for our sample (e.g., radio, submillimeter, and optical flux limits and spectroscopic incompleteness) may have influenced the observed properties.

Figure 1 shows our spectroscopic completeness as a function of R-band magnitude, 1.4 GHz radio flux, and 850 μm submillimeter flux. The median properties of the parent sample are $R_{\rm AB} = 25.4 \pm 1.8$, $S_{1.4\,\rm GHz} = 75 \pm 127$ μJy, and $S_{850\,\mu\rm m} = 6.0 \pm 2.9$ mJy, while the spectroscopically identified population has $R_{\rm AB} = 24.6 \pm 1.7$, $S_{1.4\,\rm GHz} = 78 \pm 106$ μJy, and $S_{850\,\mu\rm m} = 5.7 \pm 3.0$ mJy. As expected, our spectroscopic sample is biased toward the optically brighter galaxies (the median R-band magnitude for the unidentified spectroscopic targets is $R_{\rm AB} = 26.1 \pm 1.2$), but there is no discernible difference in the submillimeter or radio distributions (which are effectively decoupled from the rest-frame UV emission). This suggests that the long-wavelength properties of our spectroscopic sample are likely to be representative of the more general submillimeter population.

A crucial feature of the present study is that by analyzing only the radio-identified SMGs we are considering only part of the total SMG population. We must therefore determine the influence of the resulting selection function before drawing wider conclusions about flux-limited submillimeter samples.

About 65% of the bright (>5 mJy) SMG population are detectable in the deepest radio maps obtainable with the VLA (Ivison et al. 2002; Chapman et al. 2003c; Wang et al. 2004; Borys et al. 2004). Greve et al. (2004) and Ivison et al. (2005) have recently suggested that the fraction of bright SMGs, robustly confirmed at both 850 and 1200 μm, that are detected in the radio may be even higher: $\sim$80%. The remaining $\sim$35% of SMGs *not* detected in our radio maps (and therefore not included in the distributions of Fig. 1) could in principle have a wide range of properties and redshifts.

We can elucidate the effects of our radio preselection further by considering the spectral energy distributions (SEDs) of SMGs in more detail. A range of possible SEDs for a canonical 6 mJy radio SMG at $z = 2.4$ with a 50 μJy radio counterpart is shown in Figure 3. The top panel shows SEDs (Dale & Helou 2002) spanning a range of dust temperatures, all with the same radio flux and therefore comparable FIR luminosities. The range

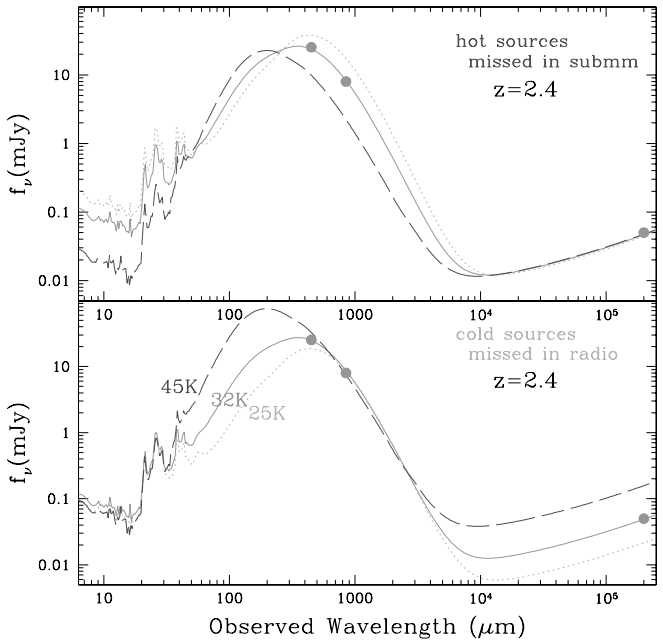

FIG. 3.—Possible SEDs describing the emission from a typical SMG, lying near the median redshift for the model-corrected sample ($z = 2.4$), with flux densities of 6 mJy at 850 μm and 50 μJy at 1.4 GHz (near our radio detection limit). Superposed are SED templates at three dust temperatures (25, 32, and 45 K) spanning the typical range observed in the SMGs. *Top*: SEDs normalized to the radio point to emphasize how sources with hotter characteristic dust temperatures and lower implied dust masses are missed in the submillimeter at $z \gtrsim 2$. *Bottom*: SEDs normalized to the 850 μm point, highlighting how sources with cooler characteristic temperatures are undetectable in the radio at the redshifts higher than the sample median.

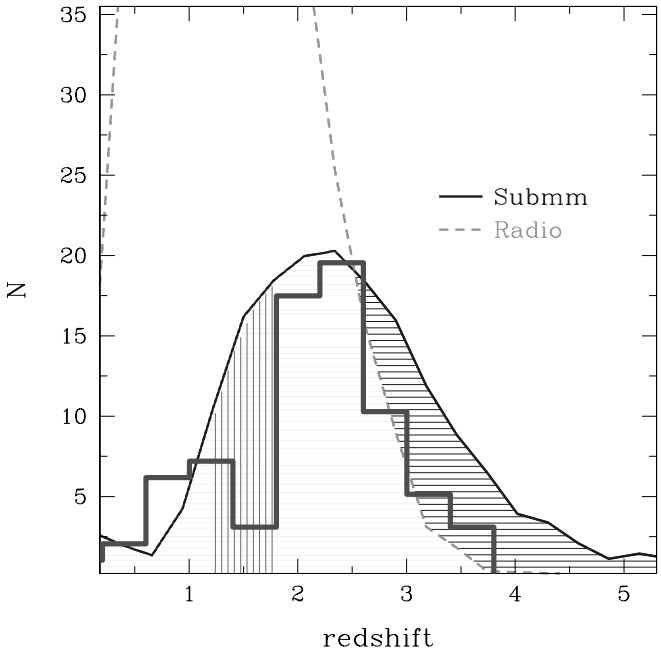

FIG. 4.—Redshift distribution of our SMG sample (*histogram*). To interpret the likely effects of the sample selection on this distribution, we plot predicted model redshift distributions for SMGs with $S_{850\,\mu m} > 5$ mJy (*solid line*) and radio sources with $S_{1.4\,GHz} > 30$ μJy (*dashed line*) based on the evolutionary models of Blain et al. (2002) and a family of long-wavelength SEDs tuned to reproduce the distribution of submillimeter/radio flux ratios (Chapman et al. 2003b; Lewis et al. 2004). The region shaded with horizontal lines highlights the redshift range in which no strong line features enter the observable wavelength range of LRIS. The region shaded with vertical lines identifies the distribution of that proportion of the population we expect to miss due to our radio flux limit.

in dust temperatures depicted is less than a factor 2 but results in close to a factor 10 range in submillimeter flux (see Blain et al. [2002, 2004a] for additional details of this selection effect). As a consequence, the hottest SED (with the lowest implied dust mass) shown in Figure 3 (with a characteristic temperature of 45 K) falls below the SCUBA detection threshold in our sample of 3 mJy.

This trend becomes more dramatic at lower redshifts: by shifting the SED templates to shorter wavelengths, it becomes apparent that only the coolest sources can be detected above our $\sim$3 mJy submillimeter flux limit. By contrast, the selection bias vanishes at higher redshifts; increasingly hotter sources become detectable with SCUBA above our radio limit ($\sim$30 μJy in the typical field).

However, our requirement of a radio detection to pinpoint the spectroscopic counterpart of the submillimeter source means that the opposite selection bias comes into play in our sample (Fig. 3, *bottom*); the coldest SMGs at $z = 2.4$ lie below our radio flux limit. This bias becomes an increasing concern at higher redshifts where warmer SMGs fall beneath our radio limit. We quantify the influence of our radio selection using knowledge of the range of observed SMG SED properties in § 4.1.

The observed redshift distribution in Figure 4 illustrates succinctly how the radio-undetected SMGs may relate to our radio SMG sample in this context: we expect to miss sources lying between the submillimeter and radio model curves because of our requirement of a radio detection to pinpoint the host galaxies. The radio-undetected minority of the submillimeter population is likely to overlap significantly in redshift with our present radio SMG sample. These galaxies would have characteristic dust temperatures that are typically cooler than the radio-detected galaxies at their redshifts [via the $(1 + z)$-T_d degeneracy]. Figure 4 shows that the two populations begin to overlap significantly at $z \sim 2.5$. A well-studied example of a radio-undetected SMG in this redshift range is the extremely red SMM J04431+0210 identified by Smail et al. (1999); the redshift of this galaxy was measured as $z = 2.51$ by Frayer et al. (2003) and confirmed beyond doubt as the submillimeter source through the detection of molecular gas in the CO (3–2) line by Neri et al. (2003).

3.2. *Ambiguous Radio Counterparts to Submillimeter Sources*

There are a number of other issues associated with the identification process that need to be considered. In particular, we note that the radio positions of a handful of sources lie very near ($<2''$) an obviously low-redshift galaxy. These galaxies are unlikely to be related to the submillimeter-emitting source, as should be apparent once the complete range of the galaxy and submillimeter source properties (radio luminosity and colors) are considered. Instead, we believe that these low-redshift galaxies are in fact lensing the background submillimeter sources. Detailed discussions of two of these systems can be found in Chapman et al. (2002c) and Dunlop et al. (2004). There are five such galaxies in our total sample, and we have not included these in the catalog of 73 submillimeter sources with robust redshifts, as we believe that the foreground galaxies are not the correct identifications for the submillimeter sources. In three of these cases there is evidence from near-IR imaging of faint *K*-band galaxies lying closer to the radio position than the galaxy that was spectroscopically observed. These submillimeter sources are particularly difficult to study (or even target) optically, and we may have to wait for blind CO line searches at millimeter wavelengths to determine their redshifts. For completeness, we include these galaxies in our identification table

but flag them as probable lenses and do not include them in any of our subsequent analysis.

We note that there are examples of low-redshift ($z < 1$) galaxies in which the radio emission is coincident with the spectroscopically targeted counterpart (within the relative astrometric errors), and we consider these to be the correct identifications and include them in our sample and analysis. These galaxies have inferred dust temperatures that appear cold relative to similarly luminous, local *IRAS* galaxies (Chapman et al. 2002d; Blain et al. 2004b).

In addition to the ambiguity in the small number of cases in which radio sources lie close to bright, foreground galaxies, Ivison et al. (2002) have demonstrated that roughly 10% of radio SMGs have more than one radio source within their submillimeter error circle (8″ diameter, derived on the basis of Monte Carlo simulations and through comparison with the robust identifications of SMGs in Smail et al. 2002). Taking a well-studied example from the literature: SMM J09431+4700 (Ledlow et al. 2002) represents a striking case of an SMG with two probable radio counterparts (denoted H6 and H7). Ledlow et al. (2002) obtained a spectroscopic identification of $z = 3.35$ for the optically brighter radio source, H6. Nevertheless, both radio sources were detected in the 1 mm continuum from the IRAM PdB (Tacconi et al. 2005), confirming that both contribute to the measured 850 μm flux. A search for CO emission in the system at the redshift of H6 failed to detect any molecular emission from this galaxy but did detect a massive gas reservoir in the optically fainter source, H7, confirming that both galaxies lie at the same redshift (Neri et al. 2003).

We find eight examples of multiple radio counterparts to submillimeter sources in our sample (noted in Table 2). In these cases we have taken spectra of all of the radio sources. In three cases (SMM J123621.27+621708.4, J123616.15+621513.7, and J163650.43+405734.5) we obtained a spectroscopic identification for one radio source but failed on the second. In three cases (SMM J105200.22+572420.2, J123707.21+621408.1, and J123711.98+621325.7) we confirmed that both radio sources lie at the same redshift to within 1000 km s^{-1}. And in the final two cases (SMM J105238.26+571651.3 and SMM J105225.90+571906.8) we found one radio source at high redshift ($z > 2$) and the other at $z < 0.5$. In these latter two cases, we assume that the high-redshift source is the correct identification, since its significantly greater radio luminosity suggests a dominant contribution to the submillimeter emission. However, detailed multiwavelength follow-up may reveal that the low-redshift radio source also contributes significantly to the submillimeter luminosity.

Even when only a single radio counterpart exists, the optical identifications are not always unambiguous—with two optical counterparts within the radio error circle, or $\sim$1″ offsets from the radio to optical identification. This affects only a small fraction of our sample (four SMGs, or $\lesssim$5%). Again, we have attempted to obtain redshifts for all components, but the sample is not complete in this respect (two possible counterparts remain to be observed spectroscopically). For the $\sim$10% of cases in which the optical identification is slightly offset from the radio (noted in Table 2), the optical source is sometimes extended and overlaps the radio source in lower surface brightness extensions. In these cases we are confident that we have identified the correct counterpart, although we have not necessarily characterized the source of the bolometric emission in the Keck spectrum. Chapman et al. (2004) address some of these issues through higher spatial resolution radio and optical imagery, whereas Ivison et al. (2005) examined the detailed identifications of SMGs in a robust sample within one of our survey fields. We comment on individual objects are subject to any of these identification issues in Table 2.

3.3. *Redshift Distributions*

The redshift distribution of our submillimeter galaxy sample (Fig. 4) displays a marked peak at $z \sim 2.0$–2.5, with an apparent dip in the distribution at $z \sim 1.5$ that is almost certainly a result of our failure to efficiently identify redshifts for SMGs at $z = 1.2$–1.8 where no strong spectral features fall into our observational windows. The decline in the numbers of SMGs at low redshifts is due to a combination of the submillimeter selection function and the intrinsic evolution in the population (e.g., Blain et al. 1999a). At high redshifts, our requirement of a radio detection (to locate the submillimeter counterpart) limits the maximum redshift detectable at our radio survey depths: a radio flux limit of 30 μJy yields detections of typical temperature and luminosity SMGs at $z < 3.5$.

We describe the selection effects using an evolutionary model that accounts for the dust properties of local galaxies with a range in template SEDs and that has been tuned to fit the submillimeter/radio flux distribution (Chapman et al. 2003b; Lewis et al. 2004). The model takes the local FIR luminosity function and evolves it in luminosity with increasing redshift following the functional form given in Blain et al. (2002). The functional form of the pure luminosity evolution function in this model is given as $g(z) = (1+z)^{3/2}\mathrm{sech}^2[b\ln(1+z) - c]\cosh^2 c$. The values of b and c in this function, which remain consistent with our observed redshift distribution [after filling in the redshift desert as described in this section, and assuming 1 σ Poisson error bars on the $N(z)$ histogram], are $2.10^{+0.30}_{-0.40}$ and $1.81^{+0.21}_{-0.37}$, respectively. The range of parameters effectively shifts the z_{peak} of the peak evolution function such that $z_{\mathrm{peak}} = 1.8^{+0.7}_{-0.3}$.

We plot the predicted redshift distributions for all SMGs with $S_{850\,\mu\mathrm{m}} > 5$ mJy and all radio sources with $S_{1.4\,\mathrm{GHz}} > 30$ μJy. We expect to miss sources lying between the submillimeter and radio model curves because of our requirement of a radio detection to pinpoint the host galaxies. The galaxies in this region represent 35% of the integral under the submillimeter curve (Fig. 4), in agreement with the proportion of radio-unidentified SMGs (e.g., Ivison et al. 2002; Chapman et al. 2003b). The combination of selection functions described by the model curves is clearly in good agreement with the observed redshift distribution.

Contrasting the predicted and observed redshift distributions, we would estimate that the dip due to spectroscopic incompleteness at $z \sim 1.5$ affects around 20% of our parent sample—this is close to the 26% spectroscopic incompleteness estimated for the total sample in § 3.3—suggesting that most of this arises from the so-called redshift desert. The influence of the radio selection produces an increasing incompleteness compared with the original parent sample at $z \gtrsim 2.5$. The model predicts that these missing galaxies lie at somewhat higher redshifts than our radio/SMG sample but still overlap significantly. Under this model scenario, less than 10% of SMGs lie at $z \geq 4$, where we have no identified members of the population in our survey. The observed radio SMG $N(z)$ (accounting for incompleteness in the spectroscopic desert) can be reasonably approximated by a Gaussian with a central redshift of $z = 2.1$ and a sigma of 1.2, while the model submillimeter-only $N(z)$ is fitted by a Gaussian with a central redshift of $z = 2.3$ and a sigma of 1.3.

In §§ 4.4 and 5 we attempt to combine all the observational information on the SMG population to confirm the fraction of SMGs that could plausibly lie at very high redshifts. Nevertheless, we reiterate that our survey gives access to the majority

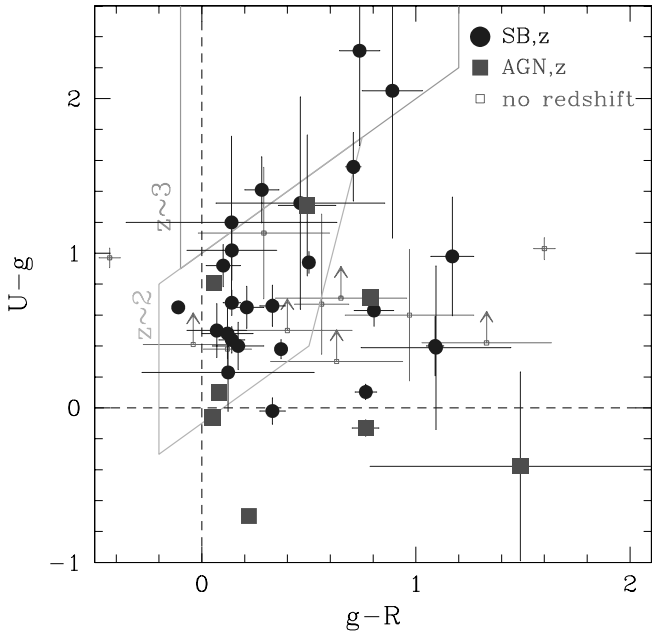

FIG. 5.—Observed frame $(U-g)$-$(g-R)$ color-color diagram for radio SMGs in the HDF-N and Westphal-14hr fields, for which deep photometry exists. Circles depict SMGs with redshifts, squares show those galaxies with AGN spectra, and small squares denote radio SMGs without spectroscopic identifications. Most of these latter category have only a lower limit on their $U-g$ colors. The color regions corresponding to $z\sim3$ (upper region) and $z\sim2$ (lower region) selection are shown (Steidel et al. 2004). All colors are on the AB scale.

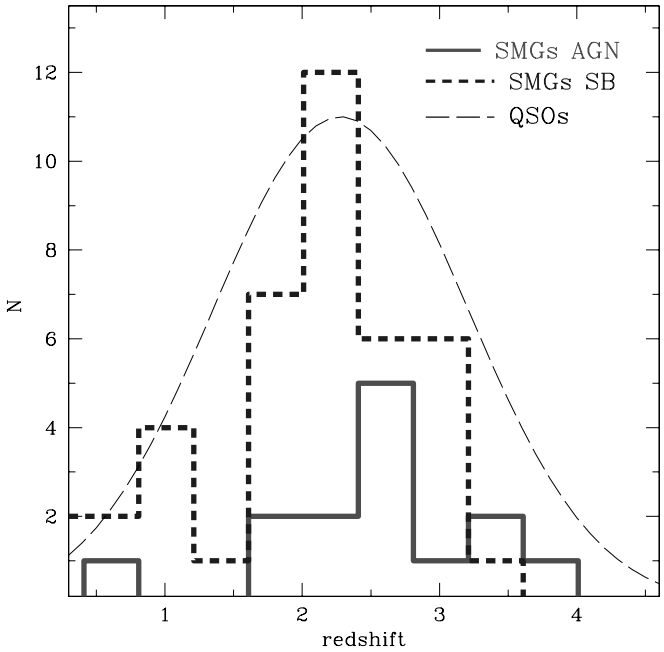

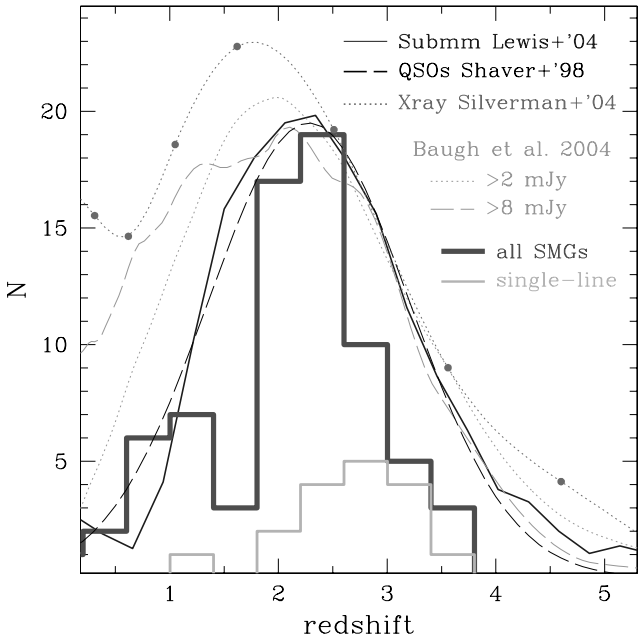

FIG. 6.—*Top*: Comparison of $N(z)$ for radio SMG with obvious AGN signatures with those without (which we denote starbursts). The $N(z)$ for a radio-selected sample of quasars unbiased by extinction (Shaver et al. 1998) is shown as a dashed curve. *Bottom*: The $N(z)$ for radio SMGs with those SMGs which were first identified in the UV spectroscopy from a single-line (Lyα in all cases except one) highlighted as a separate histogram. The SMGs are compared with the Lewis et al. (2004) model for 850 μm sources, the Shaver et al. (1998) radio-selected sample of quasars unbiased by extinction (comparable to the 2dF quasar evolution from Boyle et al. 2000 and Croom et al. 2004), and the Silverman et al. (2005) sample of *Chandra* X-ray–selected AGNs. Models of Baugh et al. (2004) for >8 mJy SMGs and >2 mJy SMGs normalized to equal numbers of sources in each $N(z)$ are also superposed.

(∼70%) of the bright (∼6 mJy) SMG population and so allows us to derive representative properties for the bulk of this important population.

It is interesting to divide the SMG sample based on the spectroscopic classifications of the members. Quasars (Shaver et al. 1998; Boyle et al. 2000; Silverman et al. 2005) and LBGs (Steidel et al. 1999; Lehnert & Bremer 2003; Giavalisco et al. 2004) show very different evolution histories from $z=1$–6. Similarly, Haarsma et al. (2000) and Cowie et al. (2004) have studied the evolution of lower redshift ($z=0$–1) faint microjansky radio sources, finding strong evolution and differing evolution for subsets of this population depending on whether their rest-frame optical/UV spectra show AGN or star formation signatures. As the top panel of Figure 6 demonstrates, the redshift distribution of the SMGs does not depend strongly on the level of AGN activity apparent in their rest-frame UV spectra. Moreover, the form of the redshift distribution for the radio/SMG population (Fig. 6, *bottom*) is very similar to that seen for quasars (Shaver et al. 1998; Silverman et al. 2005), selected in any of the optical, X-ray, or radio wavebands, and different from than that seen for UV-selected galaxies. We placed the data from Silverman et al. (2005) on Figure 6 (*bottom*) by dividing each of their points by the appropriate comoving volume element in our adopted cosmology and connecting the points with a spline fit. Only by adopting very contrived redshift distributions for the additional 35% of the SMG population that is not currently identified in the radio (Fig. 5) is it possible to make the SMGs redshift distribution differ radically from that seen for quasars. We explore this point in more detail in § 4.4. We also highlight in Figure 6 (*bottom*) those SMGs that were first identified in the UV spectroscopy from a single line (Lyα in all cases except one), and we note again that 50% of these sources have been confirmed at the correct redshift through near-IR spectroscopy of the Hα or [O III] λ5007 lines. These single-line identifications reflect the higher redshift tail of our measured $N(z)$, consistent with the generally brighter optical continuum magnitudes of the $z\sim2$ sources over the $z\sim3$ sources.

It is also interesting to study the $N(z)$ as a function of 850 μm luminosity. Model predictions of the $N(z)$ for 850 μm–selected galaxies have been presented by Baugh et al. (2004).

In Figure 6 (*bottom*) we superposed their model $N(z)$ for SMGs with $S_{850\,\mu\mathrm{m}} > 8$ mJy and $S_{850\,\mu\mathrm{m}} > 2$ mJy, the latter being dominated by the $\sim$2 mJy sources because of the steep 850 μm counts. Their models are normalized to have the same number of sources in the $N(z)$ integral. Baugh et al. (2004) find that the median redshift of the SMGs does not change significantly over the 2–8 mJy flux range.

We can divide our observed SMG sample into equal number bins with $S_{850\,\mu\mathrm{m}} > 5.5$ mJy and $S_{850\,\mu\mathrm{m}} < 5.5$ mJy, as shown in Figure 6 (*bottom*). Our submillimeter *brighter* galaxies (median $S_{850\,\mu\mathrm{m}} = 7.9$ mJy) clearly lie preferentially at higher redshifts, with a median redshift of $z = 2.45$ (interquartile ± 0.35), compared with the submillimeter fainter galaxies (median $S_{850\,\mu\mathrm{m}} = 4.7$ mJy) with median $z = 2.01$ (interquartile ± 0.61). At face value, this result disagrees with the Baugh et al. predictions. As we might expect from a radio flux–limited survey, the radio properties of the submillimeter bright and faint samples are indistinguishable (submillimeter bright: $S_{1.4\,\mathrm{GHz}} = 74 \pm 27$ μJy, submillimeter faint: $S_{1.4\,\mathrm{GHz}} = 76 \pm 29$ μJy), suggesting that our radio selection criterion is at the root of the discrepancy with the Baugh et al. model. For example, if the overall properties of submillimeter-selected galaxies were similar for the $S_{850\,\mu\mathrm{m}} \sim 2$ and $\sim$8 mJy samples (in particular the FIR-radio correlation), as in the models of Baugh et al. (2004), we would expect to miss more of the $S_{850\,\mu\mathrm{m}} \sim 2$ mJy sources at higher redshifts because of the radio detection criterion. As we see in § 4.1, these properties imply that the submillimeter-bright and -faint subsamples coincidentally have indistinguishable distributions in dust temperature. Thus, while at face value these results appear to imply that more bolometrically luminous SMGs tend to lie at higher redshifts, consistent with a strong luminosity evolution (see § 4.2), strong selection effects are at present in our submillimeter/radio sample, and we must exercise caution in our interpretations of these trends.

3.4. *Optical Spectroscopic Characteristics of SMGs*

With 73 spectral identifications, we have the statistics to begin exploring the range of galaxy types in the SMG population (Table 4). Eighteen of our galaxies (25% of the sample) show clear AGN signatures in their spectra: three of these are broad-line AGNs, with the remaining 15 being narrow-line AGN. A larger fraction of SMGs (30/73) have rest-frame UV spectroscopic characteristics similar to those of star-forming galaxies, without any identifiable AGN signatures. The remaining 25 spectroscopically identified SMGs in our sample have redshifts that are identified primarily through a strong Lyα line and do not have the continuum signal-to-noise ratio (S/N) to rule out weak AGN features. However, we note that the limits on their Lyα to [C IV] λ1549 line ratios are generally consistent with those expected for starbursts. We stress that the relatively high completeness of our survey relies in part upon the surprising strength of the Lyα emission from these supposedly highly obscured galaxies. The flux of the Lyα emission line indicates that Lyα photons can readily escape from submillimeter-selected galaxies and suggests that they may have very patchy and inhomogeneous dust distributions (see Neufeld 1991; Chapman et al. 2004).

The high fraction of UV–emission-line galaxies in our sample (38/56 of those at high enough redshift to detect Lyα, or 68%) is striking as compared with rest-frame UV-selected galaxies at $z = 2$–3, given the similarity of their broadband colors (as is discussed below). The Lyman break galaxy (LBG) population (Steidel et al. 2003) at $z \sim 3$ shows strong Lyα emission in only 25% of the cases (Shapley et al. 2003), and their lower redshift counterparts, the BX/BM galaxies, show an even lower fraction with Lyα emission (Steidel et al. 2004). In part, however, this might be a selection effect resulting from the difficulty of measuring absorption-line redshifts for the fainter SMGs (from the total spectroscopically observed sample of 98, there are 38/81, or 47%, Lyα emission-line systems in the total sample of spectroscopically observed galaxies, again excluding the spectroscopically identified SMGs at redshifts too low to detect Lyα, $z < 1.7$). If we only consider the subsample of SMGs with $R_{\mathrm{AB}} < 23.5$ (21 galaxies), for which our spectroscopic identifications are effectively complete, Figure 1, 10/21 are at $z > 1.7$ to measure Lyα. And 8/10 of these have Lyα in emission.

TABLE 4

Radio SMG Spectral Classification Statistics

Class	Number	Percentage (%)
Successful spectroscopic IDs	(73)	
UV-emission line	38/56	68
AGN lines (C IV, etc.)	18/73	25
Broad-line AGN	3/73	4
Identified primarily through Lyα	25/73	34
Total spectroscopic sample	(98)	
Lyα emitting	38/81	47
AGN characteristics	18/98	18
Star-forming galaxies	30/98	31
Difficult to classify	25/98	25
Spectroscopically unidentified	25/98	26

In addition to the 73 SMGs with robust redshifts, there are 25 of the optically faintest radio SMGs for which we have spectroscopic observations but failed to measure a redshift. None of these sources appear to exhibit strong, narrow emission lines in the observed UV/optical wavebands. There are two possible redshift ranges in which this population could reside. First, they may lie at $z \sim 1.2$–1.8, where no strong emission or absorption features fall in the sensitive range of the LRIS spectrograph. Alternatively, they may lie within the redshift distribution of our spectroscopically identified sample but have spectra that are characterized by absorption lines, in particular absorbed Lyα. As these tend to be among the faintest sources in the sample (Fig. 1), the S/N in their spectra is often lower than for our successful spectroscopic identifications.

To summarize, from the 98 radio SMG for which we obtained spectroscopic observations, 18% show obvious AGN characteristics, 31% are apparently star-forming galaxies, 25% are difficult to classify but remain reasonable candidates to be star-forming galaxies, and 26% are spectroscopically unidentified and so are unlikely to be strong AGNs at $z < 1.2$ or $z > 1.8$ (although they could be star-forming galaxies with weak/absent emission lines at almost any redshift). Assuming that the redshift distributions for the AGN and starburst populations are comparable, including those spectrally unclassified SMGs at $z = 1.2$–1.8 with AGN spectral signatures is unlikely to increase the fraction of such galaxies in the total sample above 25% (see § 3.5). This is a lower AGN fraction than suggested by either the identification of X-ray counterparts with QSO- or Seyfert-like luminosities ($\gtrsim$36%; Alexander et al. 2002) or Hα line widths of $\geq$500 km s^{-1} (46% $\pm$ 14%; Swinbank et al. 2004). We conclude that perhaps a third of SMGs identified as apparently star-forming or unclassified based on their rest-frame UV spectral properties are likely to host unidentified (most likely obscured) AGN.

3.5. *Optical Photometric Properties of SMGs*

In the deepest ground-based optical images the majority of SMGs are detected in most or all wavelengths observed. This is particularly true in the HDF-N and Westphal-14 hr/SSA22 fields for which extremely deep *UBR* imaging from Subaru/Suprime-Cam and Kitt Peak/MOSAIC imaging (Capak et al. 2004) and deep U_n, g, and R_s (hereafter *UgR*) images (Steidel et al. 2003) exist, respectively.

In Figure 5 we show the $(U-g)$-$(g-R)$ color-color diagram for those radio SMGs with robust spectral identifications and redshifts $z > 1.5$. We compare these with the $z \sim 3$ and ~ 2 selection criterion presented in Steidel et al. (2004). Color transformations were determined between filter bands by matching the catalogs of $z \sim 2$ and ~ 3 galaxies lying in the extended HDF region and rederiving the colors from the Capak et al. images. The *UBR* AB magnitudes of the Steidel et al. (2004) BX/BM galaxies in the HDF region were first measured using the Suprime and MOSAIC images of Capak et al. (2004). A new BX color-selection box was then defined empirically for these *UBR* filters. The median offset in magnitudes $U - U_n$, $B - g$, and $R - R_s$ (0.22, 0.13, and 0.04) was then applied to our measured *UBR* magnitude for the SMGs.

Many of the SMGs ($\sim$65%) lie well within the $z \sim 2$ color selection region from Steidel et al. (2004), in accord with their spectroscopic redshifts. Approximately 30% of the galaxies are too red in $(g-R)$ to be selected by the rest-frame UV criterion, possibly because of dust extinction. Smail et al. (2004) present a complete study of the extinction properties of SMGs using near-IR photometry. The relative classification of AGN and SB populations of SMGs suggests that the strong emission-line AGNs tend toward redder $g-R$ colors with a median $g-R = 0.5 \pm 0.1$, compared with the non-AGN sample with $g-R = 0.4 \pm 0.1$.

We also show the colors of sources for which we failed to obtain spectroscopic redshifts. Many of these are detected near the limit of the photometry in the *BR* passbands but are undetected at *U* and are thus shown as lower limits in $U-g$ in Figure 5. Many of these galaxies also lie within the $z \sim 2$ color selection region but with much larger uncertainties. This provides some additional evidence that the radio SMGs for which we were unable to obtain spectroscopic identifications likely span a similar range in redshift to those with robust identifications.

While the colors of many SMGs appear consistent with the BX selection, a significant fraction ($\sim$50% of the total radio SMG sample, and $\sim$30% of the spectroscopically identified radio SMGs) are too faint to be selected in typical BX/LBG samples (typically $R_s < 25.5$; Steidel et al. 2004). Of the SMGs depicted in Figure 5 (having $z > 1.5$ and lying in the HDF, Westphal-14, and SSA22 fields), the median and average quartile distribution of the total sample is $R = 25.3 \pm 0.8$, while the distributions for the spectroscopic successes and failures are, respectively, $R = 24.9 \pm 0.9$ and 25.7 ± 0.4.

This exercise suggests that deep optical imaging may provide reliable photometric redshifts, which are immune from the temperature uncertainty that plagues simple radio/submillimeter photometric redshift estimates (see § 3.6). Using the HYPER-Z software (Bolzonella et al. 2000) for this sample and their *UgRiK* magnitudes, we derive photometric redshifts with a median error of $\sim$30% (see also Smail et al. 2004).

3.6. *Submillimeter/Radio Indices and Redshifts*

In Figure 7, we show the ratio of submillimeter to radio flux as a function of redshift for our SMG sample. We also assess the locations of the eight radio-identified SMGs from the literature with robust redshift identifications. The variation of the submillimeter/radio flux ratio with redshift is the basis for the Carilli-Yun redshift indicator (Carilli & Yun 1999, 2000). However, this diagram also depicts the variation in SED properties spanned by the SMGs, although these are subject to considerable selection effects. This figure is in essence a depiction of the joint evolution in the FIR/radio correlation and the range in dust properties in luminous galaxies (see § 4.1).

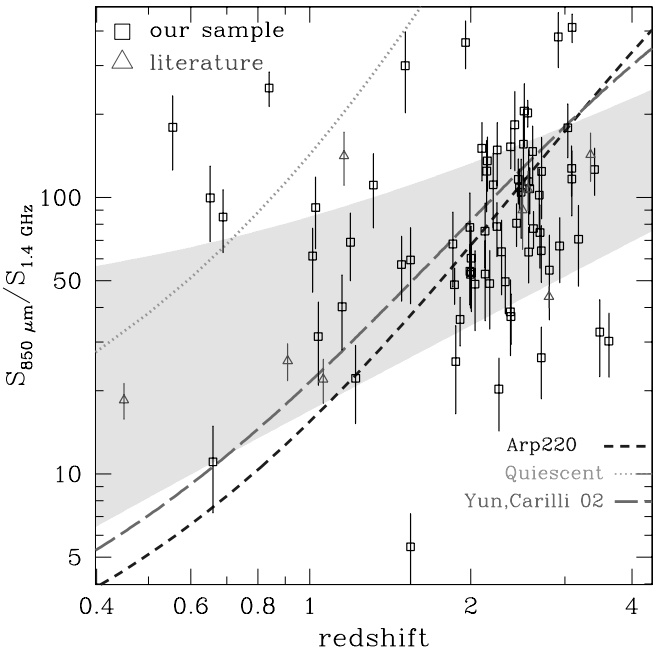

FIG. 7.—Plot of $S_{850\,\mu m}/S_{1.4\,GHz}$ vs. redshift for the radio SMGs with spectroscopic redshifts from our sample and from literature sources not lying within our fields (Smail et al. 2002, 2003b; Chapman et al. 2002d). The shaded region shows the $\pm 1\ \sigma$ envelope of the rms dispersion calculated in three redshift bins containing equal numbers of SMGs. The predicted variation in flux ratio for three SEDs are superposed: Arp 220, a quiescent spiral galaxy (such as the Milky Way) and an empirically derived track from the literature (Yun & Carilli 2002).

We superpose the tracks of two galaxy classes on Figure 7, representative of quiescent spirals, such as the Milky Way, and ultraluminous galaxies ($L_{bol} \sim 10^{12}\ L_\odot$), such as Arp 220. We also show the track derived by Yun & Carilli (2002) using a compilation of low- and high-redshift galaxy samples. This latter track and other similar ones from the literature (Dunne et al. 2000; Barger et al. 2000) have been widely used to estimate SMG redshifts. If the SMGs were to represent a population with a narrow range of spectral energy distributions, then we would expect them, on average, to trace a well-defined track in the CY diagram. As they appear to be widely scattered at a fixed redshift (an order of magnitude range in the flux ratio at $z \gtrsim 1$), a natural interpretation is that they span a range in SED shapes (characterized by T_d; § 4.1). We note that our radio selection criteria may bias us toward identifying objects with enhanced radio-to-FIR emission (similar to the local *IRAS* galaxy Mrk 231, whose AGN contributed a comparable radio luminosity to the starburst in this galaxy). The preferential inclusion of these systems in our radio-identified sample would lower the typical flux ratio of the high-redshift SMGs in our $S_{850\,\mu m}/S_{1.4\,GHz}$ diagram by about 0.3 dex. Yun et al. (2001) suggest that such galaxies could make up a few to 10% of SMGs, implying at most a small bias.

To quantify the dispersion of $S_{850\,\mu m}/S_{1.4\,GHz}$, we divide the sample in redshift into three bins containing equal numbers of

SMGs and plot the 1 σ dispersion envelope on Figure 7. Clearly a large dispersion in SED properties is spanned by our SMG sample, with a preference for the warmer templates (the Arp 220 rather than quiescent models). The trend of submillimeter/radio flux ratio with redshift is much flatter than the rapidly rising template tracks and can be parameterized by

$$S_{850\ \mu\mathrm{m}}/S_{1.4\ \mathrm{GHz}} = 11.1 + 35.2z,$$

with an average rms dispersion in the range $z = 1$–4 of $\sigma(S_{850\ \mu\mathrm{m}}/S_{1.4\ \mathrm{GHz}}) \sim 40$. The shallow slope of this trend greatly increases the error in the redshift estimate for a given submillimeter/radio ratio. This behavior can be partially explained by the fact that lower redshift sources tend to be lower luminosity and cooler, following the weak local correlation between temperature and luminosity (Chapman et al. 2003b). However, this should be only a slight effect. The selection criteria in the submillimeter/radio are mainly responsible for the narrow range of submillimeter/radio values observed, and almost no discrimination is achieved for individual source redshifts, where $\Delta z \sim 1$ (see also Blain et al. 2004b). It should be noted that a purely submillimeter-selected sample should show an even wider range in submillimeter/radio flux ratios than our sample—which already demonstrates that the range of SED properties in the SMG population render simple photometric redshift estimates too imprecise to be useful for predicting redshifts for individual galaxies (e.g., Aretxaga et al. 2003; Efstathiou & Rowan-Robinson 2003; Wiklind 2003).

The Carilli & Yun redshift estimator has been extensively employed (Smail et al. 2000; Barger et al. 2000; Chapman et al. 2001b, 2002a; Ivison et al. 2002), but until now it has not proved possible to critically compare it with a large sample of SMGs with precise redshifts. Perhaps surprisingly, the median redshift predicted for the SMG population using $S_{850\ \mu\mathrm{m}}/S_{1.4\ \mathrm{GHz}}$ ($z \sim 2.5$) has turned out to be remarkably close to the value we derive. In part this is because, on average, the SMGs have SEDs similar to local ULIRGs and so the average properties derived for the population are not too far wrong. However, this effect is further aided by the relatively narrow redshift distribution seen for SMGs—which limits the intrinsic dispersion in the median redshift for the population.

4. DISCUSSION

4.1. *Dust Temperatures and Luminosities*

Having constrained the redshift distribution and basic observable properties of the SMGs, our next goal is to study the distribution of their SED properties and bolometric luminosities.

Studies of local and moderate redshift galaxies in the radio and submillimeter wavebands suggest that variations in both the dust properties and the empirical relation between the FIR luminosity (L_{FIR}) and 1.4 GHz radio (Helou et al. 1985; Condon 1992) affect the observed radio flux from a SMG. The dust properties in luminous infrared galaxies such as SMGs are potentially very complicated, requiring many parameters for a complete characterization. However, Blain et al. (2002) demonstrated that the characteristic dust temperature (T_d, the best single-temperature graybody fit to the SED) is the main parameter influencing the ratio of submillimeter to radio emission and hence the observed radio flux. Since we only have a redshift and two photometric points in the relevant region of the SED (850 μm and 1.4 GHz) from which to disentangle the dust properties, we thus concentrate only on the dust temperature, fixing the remainder of the dust properties at canonical values for local ultraluminous infrared galaxies (ULIRGs). In the absence of additional information for most of our sources, we adopt a dust emissivity of $\beta = 1.5$.

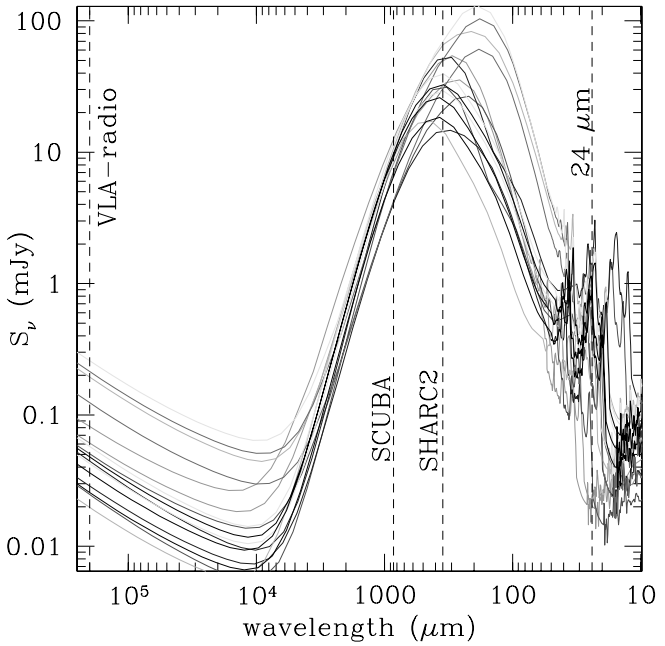

FIG. 8.—Redshifted SED templates for galaxies from Dale & Helou (2002) that are consistent with the radio and 850 μm fluxes of 16 representative SMGs from our sample. The galaxies span a range in dust properties, translating into characteristic temperatures from ~20 to ~60 K if the FIR to radio correlation holds at high redshift. We mark on the wavelengths corresponding to observations with SCUBA at 850 μm, VLA at 20 cm, SHARC-2 at 350 μm, and *Spitzer*/MIPS at 24 μm.

We therefore proceed by translating our observables (submillimeter and radio fluxes and redshift) into intrinsic physical properties, T_d and total infrared luminosity L_{TIR} (defined as the integral between 8 and 1100 μm and derivable from FIR with a small color-correction term; e.g., Dale et al. 2001). We calculate T_d explicitly by adopting a suite of dust SED templates from Dale & Helou (2002), spanning an equivalent range of T_d from 15–90 K (e.g., Fig. 8).

The templates assume the median value of the local FIR/radio relation (Helou et al. 1985), allowing a one-to-one mapping of $S_{850\ \mu\mathrm{m}}/S_{1.4\ \mathrm{GHz}}$ flux ratio to T_d. These template fits to a representative selection of galaxies from our sample are shown in Figure 8. We also assume the low-redshift FIR/radio relation to calculate L_{TIR} for our sources. Radio luminosities are calculated by first K-correcting the observed fluxes to the rest frame using a synchrotron spectrum with an index of $\alpha = -0.75$. Our adopted spectral index is supported by the small number of galaxies in our sample that have measured radio spectral indices (Ivison et al. 2002; Richards 2000). In this parametrization, the location of a galaxy with a measured redshift in Figure 7 is uniquely described by its value of T_d. In Figure 9 we plot T_d versus L_{TIR} for our SMGs; the median T_d is 36 K (12 K interquartile range) and the median $L_{\mathrm{TIR}} = 8.5^{+7.4}_{-4.6} \times 10^{12}\ L_\odot$, but note the strong correlation between observed luminosity and temperature. With our assumption of the FIR-radio relation and fitting to the observed $S_{850\ \mu\mathrm{m}}/S_{1.4\ \mathrm{GHz}}$ distribution for our SMGs, the dust temperature is approximately proportional to

$$T_d \propto \frac{1 + z_{\mathrm{spec}}}{(S_{850\ \mu\mathrm{m}}/S_{1.4\ \mathrm{GHz}})^{0.26}}.$$

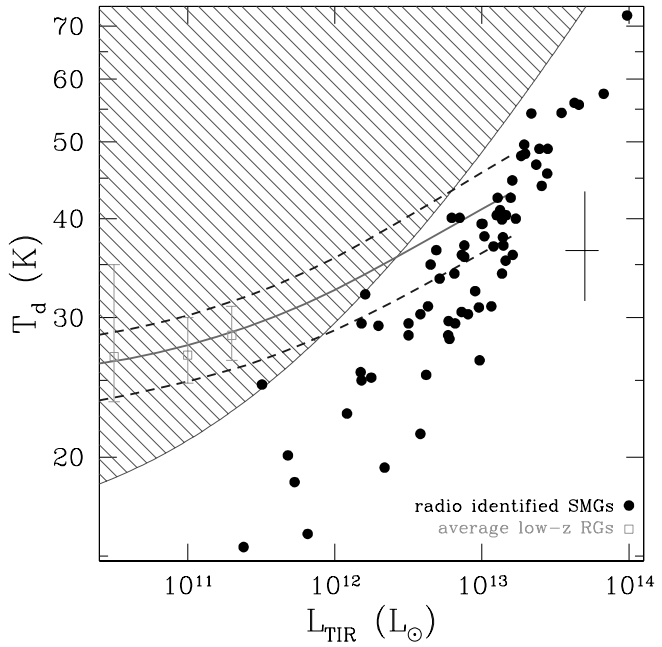

FIG. 9.—Characteristic dust temperature (T_d) vs. log of the total IR luminosity for radio SMGs with spectroscopic redshifts from our sample. We see a tight trend of inferred temperature with IR luminosity—but propose that this mostly arises from the selection criteria for our sample. The Chapman et al. (2003b) derivation of the median and interquartile range of local *IRAS* galaxies from the 1.2 Jy 60 μm catalog is shown, linearly extrapolated to 10^{13} $L_\odot$. The average T_d-values for $z = 0.3$–1 μJy radio sources from Chapman et al. (2003c) are shown and agree well with the trend from *IRAS* distribution. The submillimeter flux limit precludes detection of sources in the shaded region (shown for 3 mJy, the weakest source flux in our sample). The average error bar for galaxies in the SMG sample is shown at the median temperature of the sample, offset arbitrarily in luminosity.

Interestingly, the SMGs in our sample show no temperature dependence with submillimeter flux density. The submillimeter bright and faint subsamples (as described in § 3.5) have indistinguishable distributions in T_d: 36 ± 4 versus 37 ± 6 K (interquartile error ranges).

Two strong selection effects are at work in Figure 9. The first is the selection effect imposed by the sensitivity limit of the submillimeter observations. This is shown as a shaded region in Figure 9; galaxies with hotter dust temperatures are excluded from our sample unless they exceed a minimum luminosity. Similarly, the requirement for a radio detection removes the coldest galaxies from our sample, selectively removing objects from the region in the lower right of Figure 9. However, the dominant effect clearing out the lower right region of Figure 9 is the steeply declining high-L tail of the luminosity function (see Blain et al. 2004b for a detailed analysis). The requirement for a radio detection is the origin of the difference between the high-redshift tail of the observed redshift distribution and that predicted for a purely submillimeter flux–limited sample in Figure 4. The model suggests that a reasonable fraction of SMGs with radio fluxes below our detection limits should have redshifts in a similar range ($z \sim 2.5$–3.5) to the radio SMGs presented here but that these SMGs have a slightly cooler dust temperature (at a given luminosity) than found in our radio SMG sample.

Both our inferred dust temperatures and luminosities depend on the FIR-radio relation holding at high redshifts. Based on empirical relations of local infrared galaxies, the scatter in the FIR-radio (0.2 dex) and T_d-$L_{\rm TIR}$ relations ($\sim$0.4 dex) are expected to vary the observed submillimeter/radio flux ratio in the SMGs, producing a random uncertainty in our SMG calculations. However, it is systematic errors due to evolution of these two relations (neither of which has been measured explicitly at high redshift) that are of more concern when comparing the median properties of the SMG population with luminous, obscured galaxies in the local universe. We now discuss possible sources of error and the constraints that are available on the form of the relations at high redshifts.

One possible source of error in our estimates would come if excess radio-loud emission from an AGN was boosting the observed radio flux, which would result in $L_{\rm TIR}$ being overestimated. This emphasizes the fact that correctly interpreting Figure 9 has more to do with the range of SED types spanned by our sample as a function of luminosity. The SED variation between our SMGs could in principle arise entirely from a larger scatter in the FIR-radio correlation than that observed locally. In the extreme case, in which our entire sample would be at the same dust temperature of $T_d = 36$ K, the FIR-radio correlation would have to have a dispersion of 0.8 dex to reproduce the variation in SEDs observed in Figure 9. There are physical reasons why there could be such deviations from the correlation at high redshift. For instance, ages, differences in dust properties, magnetic field strength, or the initial mass function all are conceivable in very luminous, active young galaxies at high redshift, and all would act to increase the dispersion in the relation (see also Eales et al. 2003).

Garrett (2002) used the radio measurements of 15 μm *Infrared Space Observatory* (*ISO*) galaxies to infer that $z < 1$ infrared galaxies broadly follow the local FIR-radio relation. A more reliable test of our T_d-L estimates is the measurement of SMG SEDs at shorter submillimeter wavelengths. Figure 8 suggests that the peak of the SEDs for our SMGs lies at observed wavelengths around 350–450 μm, and hence flux measurements at these wavelengths will be particularly useful for determining the characteristic dust temperatures of the galaxies. Although the SCUBA instrument simultaneously measures 450 μm fluxes (in parallel with our 850 μm observations), our 450 μm data is typically of insufficient quality (because of the weather conditions) to usefully constrain the SEDs, failing to individually detect the vast majority of SMGs. However, stacking our 450 μm observations does verify that the FIR/radio and 850 μm points appear to predict T_d reasonably well, although calibration uncertainties at 450 μm make this a difficult measurement (see also Dunne et al. 2001). The average (inverse variance–weighted) measured flux is $S_{450\,\mu{\rm m}} = 32 \pm 6$ mJy for our SMG sample, while the median FIR-radio ratio predicted $S_{450\,\mu{\rm m}} = 41 \pm 12$ mJy. As we have noted, we do not have sufficient S/N on an object-to-object basis at 450 μm to determine how tight the correlation is.

At somewhat shorter wavelengths, A. Kovacs et al. (2005, in preparation) detected more than 10 of our sample using the 350 μm SHARC-2 camera on the Caltech Submillimeter Observatory. These results suggest that our T_d predictions are accurate to $\sim$20% (without considering systematic calibration effects of SHARC-2), corresponding to an uncertainty in the total infrared luminosity of $\sim$85% ($L_{\rm TIR} \propto T_d^{3.5}$ for $z \sim 2.2$ sources). This implies that the FIR/radio correlation can be used to predict the dust temperature of a typical SMG with reasonable precision and therefore that radio observations alone could be used to estimate FIR luminosity of a star-forming galaxy for many purposes once the spectroscopic redshift has been measured.

Figure 9 provides a complementary view of the $S_{850\,\mu{\rm m}}/S_{1.4\,{\rm GHz}}$-redshift diagram in Figure 7, with the redshift information now hidden in the luminosity and differences in $S_{850\,\mu{\rm m}}/S_{1.4\,{\rm GHz}}$ manifested as changes in T_d. Figure 9 does, however, allow for a

direct consistency check with the properties of local and moderate-redshift *IRAS* galaxies, of which our radio SMG population could represent high-redshift analogs. To provide a stepping stone to the high-redshift SMG population, we have also calculated the T_d values for $z = 0.3$–1 μJy radio galaxies (Fig. 9) from Chapman et al. (2003c) in the same manner as for our radio SMG sample, using the $S_{850\,\mu\mathrm{m}}/S_{1.4\,\mathrm{GHz}}$ ratio. These values allow us to confirm that the form of the T_d-L relation from the local *IRAS* samples appears to hold out to $z \sim 1$. Note, however, that these lower redshift radio sources are not individually detected in the submillimeter, and so the error bars are dominated by measurement errors, rather than representing a true distribution of the T_d values. The average submillimeter flux densities of these galaxies are $\sim$1 mJy, and so they fall within the shaded submillimeter flux selection region of the diagram.

Figure 9 demonstrates that the distribution of the radio SMG population appears inconsistent with the expected local T_d-L relation characterized by Chapman et al. (2003b; see also Blain et al. 2004b). The median T_d of our SMGs (36 K) is lower than the locally predicted T_d for galaxies of these luminosities (at $L_{\mathrm{TIR}} = 10^{13}\,L_\odot$ the local median is 42 K).

As we noted in § 3.6, our radio detection criterion might be expected to bias us toward galaxies with SEDs similar to Mrk 231, with radio excess over the local FIR/radio relation, which make up 10% of local *IRAS* galaxies (Yun et al. 2001). Such galaxies would be offset to *hotter* temperatures in Figure 9, in the opposite sense to the offset we see, and are therefore not likely to represent a large fraction of our SMGs. Nevertheless, the decreased median T_d (relative to the local prediction) could still be a selection effect, since we have potentially missed luminous galaxies with both hotter and colder dust temperatures through our combined radio/submillimeter selection function. Chapman et al. (2004) uncovered a sample of apparently hot and luminous galaxies (lying above our submillimeter selection boundary), whose inclusion would increase the median T_d significantly. In contrast, Ivison et al. (2005) suggested likely identifications for SMGs in our sample that lack radio detections; these galaxies would appear on Figure 9 with colder T_d than our radio SMGs. Both of these *missing* populations of luminous galaxies suggest that the true T_d scatter in high-redshift, luminous galaxies is larger than that observed locally. The scatter in the observed temperatures of our SMGs (12 K interquartile range) is already larger than observed locally (8 K interquartile range). While we note that some broadening of the local distribution is suggested for the highest-luminosity galaxies, any additional hotter or colder SMGs in the high-redshift sample would only increase the this difference in the dispersion of the two populations.

On their own our spectroscopic redshifts and radio/submillimeter photometry for radio SMGs cannot provide a complete picture of the range in SEDs spanned by the most luminous galaxies in the universe. However, the available evidence suggests that some caution should be exercised when assuming that the T_d-L properties of luminous, high-redshift dusty galaxies are identical to those at low redshifts.

TABLE 5

FIR Luminosity Function for SMGs: $z = 0.9$

$\log(L_{\mathrm{FIR}})$ ($L_\odot$)	$\log N$ (h^{-3} Mpc^{-3} decade^{-1})
11.4	$-6.04^{+0.16}_{-0.26}$
11.9	$-5.84^{+0.13}_{-0.19}$
12.4	$-6.26^{+0.20}_{-0.37}$
12.9	$-6.74^{+0.30}_{-1.70}$

TABLE 6

FIR Luminosity Function for SMGs: $z = 2.5$

$\log(L_{\mathrm{FIR}}/L_\odot)$ ($L_\odot$)	$\log N$ (h^{-3} Mpc^{-3} decade^{-1})
12.5	$-5.44^{+0.09}_{-0.11}$
12.9	$-5.29^{+0.08}_{-0.09}$
13.3	$-6.04^{+0.16}_{-0.26}$
13.7	$-6.74^{+0.30}_{-1.70}$

4.2. *The Bolometric Luminosity Function*

Estimates of radio SMG dust temperatures using the FIR-radio correlation allow the calculation of bolometric luminosities, and we can use the effective volume of our submillimeter redshift survey to construct a bolometric luminosity function in two redshift ranges at $z = 0.9 \pm 0.3$ and 2.5 ± 0.5 (Tables 5 and 6).

The 850 μm fluxes of the galaxies in our sample span a factor of 5 range, translating into a similar range in submillimeter luminosities. By including the temperature information we can estimate bolometric luminosities, which span a slightly larger range of about a factor of 10. We note again that our bolometric luminosity calculations assume that the T_d-L properties of luminous, high-redshift dusty galaxies are similar to those at low redshifts, and some caution should be exercised when interpreting the results.

Computing the raw volume densities of the radio SMGs is accomplished using the radio luminosity and an accessible volume technique, as described in Avni & Bachall (1980). We adopt a general form for the luminosity function,

$$\Phi(L)\Delta L = \sum_i \frac{1}{V_i},$$

with $\Phi(L)\Delta L$ as the number density of sources (per cubic megaparsec) in the luminosity range L–$L + \Delta L$. The accessible volume, V_i, represents the ith source in the sample, the maximum volume in which the object could be located and still be detected in our 1.4 GHz VLA maps. The sum is over all sources within the luminosity range. We then map sources to their FIR luminosity using the results of § 4.1. This procedure naturally accounts for the spectroscopic incompleteness of our survey, assuming that our spectroscopically identified sources are representative of the total population of radio SMGs. The *spectroscopic desert* has also been taken into account, since the volume between $z = 1.2$–1.8 is not included in either our $z = 0.9$ or 2.5 bins.

There are several selection effects in our samples whose influence on the luminosity functions cannot be easily quantified. The most obvious of these are the overlap with radio-unidentified SMGs and differences in radio detection rate as a function of submillimeter flux (fainter submillimeter sources are likely to have fainter radio counterparts, and our completeness in identifying radio counterparts is reduced). We have discussed the probable redshift range for the $\sim$35% of the total SMG population without radio identifications. These sources probably mostly lie at higher redshifts (Fig. 4), but they overlap with the high-redshift tail of the radio SMGs (§ 2.1), producing increasing incompleteness for the faintest and coldest sources

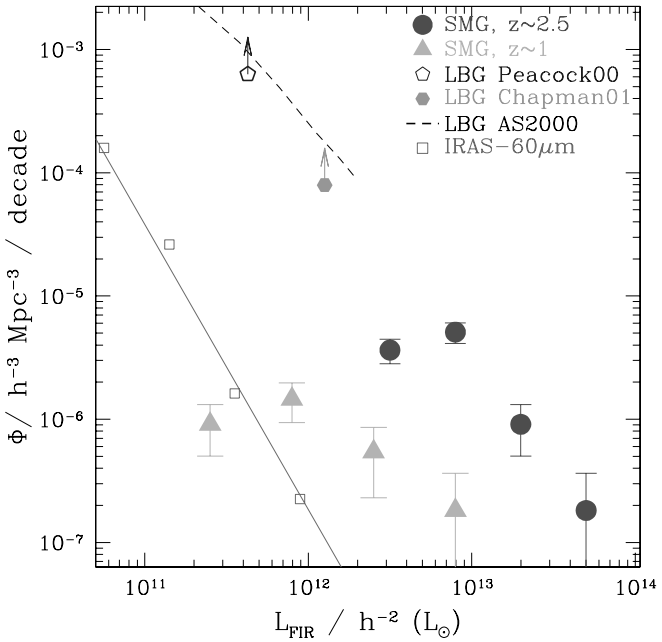

FIG. 10.—FIR luminosity functions at $z = 0.9 \pm 0.3$ and 2.5 ± 0.5. $L_{\rm FIR}$ is calculated by integrating under the template SED from the Dale & Helou (2002) catalog that best fits the submillimeter and radio fluxes of the galaxy at its measured redshift. For comparison, we show the local FIR luminosity function from Chapman et al. (2003b), constructed in a consistent manner with our $z = 2.5$ function using the Dale & Helou (2002) templates. Also shown are the submillimeter detections (>3 σ) of LBGs from Peacock et al. (2000) for SFRs $> 1\ M_\odot$ in the HDF, and for those galaxies with inferred SFRs $> 100\ M_\odot$ from Chapman et al. (2000, 2001b). For reference we plot the predicted $\Phi(L_{\rm FIR})$ for LBGs from Adelberger & Steidel (2000), which assumes the FIR/UV–β relation (where β is the UV continuum slope) of Meurer et al. (1997).

at $z > 2.5$. We may therefore have slightly underestimated the power-law slope of the luminosity function, and we note that incompleteness quickly dominates the high-redshift sample at $<10^{13}\ L_\odot$.

Comparing the number counts as a function of submillimeter flux for our sample with those from imaging surveys (e.g., as compiled in Blain et al. 2002; Borys et al. 2004) allows us to estimate our relative radio completeness with submillimeter flux. SMGs with $S_{850\ \mu{\rm m}} > 5$ mJy are detected in the radio ~6 times more frequently than 3–5 mJy sources (Chapman et al. 2002a; their Fig. 8). A correction was calculated for the effect of differential radio selection by fitting this progressive divergence of the radio SMG count from the total submillimeter count with decreasing submillimeter flux. This correction was applied to the submillimeter luminosities before translating to FIR luminosities. The result is a steepening of the slopes of the FIR luminosity function. The correction is designed to reduce the sensitivity of our luminosity function to the T_d-dependent radio selection in our faintest bins, while representing the pure radio-identified sample for the brighter SMGs.

In Figure 10, we plot our luminosity functions, parametrized by FIR luminosity ($L_{\rm FIR}$). We compare this with the equivalent distribution for local *IRAS* galaxies: the local FIR luminosity function for galaxies with $S_{60\ \mu{\rm m}} > 1.2$ Jy from Chapman et al. (2003b), which is constructed in a consistent manner to our SMG estimated function using the Dale & Helou (2002) SED templates.

The comparison in Figure 10 reveals an evolution in number density of 3 orders of magnitude for FIR-luminous galaxies locally and at $z \sim 2.5$. The slopes of the bright ends of our SMG luminosity functions are very similar to the local *IRAS* distribution, suggesting that the evolution from the local function through the $z \sim 1$ and ~2.5 functions are consistent with almost pure luminosity evolution at the bright end (although density evolution cannot easily be distinguished from luminosity evolution for the bright end of the LF; e.g., Chary & Elbaz 2001). We note, however, that density evolution is known to overproduce the submillimeter background (Blain et al. 1999a), since it would result in a very large number of low-luminosity objects. The turnover in our lowest-luminosity bins primarily reflect incompleteness in our survey, although we have attempted to correct for this as described above.

To better constrain the form of the faint end of the FIR luminosity function at $z \sim 2.5$, we need to turn to samples of galaxies selected in other wavebands. In particular, we can try to use limits on the FIR emission from UV-selected galaxies to place a lower limit on the space densities of high-redshift sources with much lower FIR luminosities than are detectable with current submillimeter facilities. The submillimeter properties of the $z \sim 3$ LBGs have been discussed by Chapman et al. (2000, 2001b), Peacock et al. (2000), and Webb et al. (2003b). Chapman et al. (2001b) and Peacock et al. (2000) report ~3 σ statistical detections of luminous LBGs at 850 μm, while Webb et al. (2003b) report a formal nondetection of the combined sample of LBGs lying within their CFRS-03 and Westphal-14 survey fields. We place the Chapman et al. (2001b) and Peacock et al. (2000) measurements on Figure 10 by assuming a $T_d = 36$ K dust template to estimate $L_{\rm FIR}$. We plot both points as lower limits because of the unknown fraction of the FIR-luminous population that is missed by the UV selection. Nevertheless, it is clear that the inferred properties of the UV-selected populations support a steep faint-end slope to the $z \sim 2.5$ FIR luminosity function, which is similar in form to that seen for *IRAS* galaxies in the local universe.

We also show on Figure 10 the inferred FIR luminosity function based on FIR/UV-β relation (Meurer et al. 1997) applied to a survey of LBGs from Adelberger & Steidel (2000) and normalized to the effective volume containing the $z \sim 3$ LBGs (Steidel et al. 1999). For the $z \sim 2$ BX/BM population (Steidel et al. 2004), stacking analysis of their radio and X-ray emission suggest that the bolometric luminosity function of Adelberger & Steidel (2000) is a reasonable representation (Reddy & Steidel 2004).

It is difficult to determine whether pure luminosity evolution can explain the dramatic increase in volume density of high-redshift galaxies with 10^{11}–$10^{13}\ L_\odot$ (based on the UV- and submillimeter-selected samples) over similarly luminous local galaxies. The high-redshift, FIR luminosity function remains poorly constrained in both low- and high-luminosity regimes. For UV-selected galaxies at high redshift it is currently very difficult to accurately estimate $L_{\rm FIR}$ (e.g., Adelberger & Steidel 2000; Reddy & Steidel 2004). In addition, it is unclear what the completeness is in $\Phi(L_{\rm FIR})$ for a UV-selected sample. The submillimeter-estimated $\Phi(L_{\rm FIR})$ at high luminosities is also poorly constrained because of incompleteness effects, which are difficult to characterize (as described above). We have already explored the extent to which the submillimeter selection itself may have significantly underestimated the total volume of luminous galaxies at high redshifts, as galaxies with hotter characteristic dust temperatures are missed by submillimeter selection (Chapman et al. 2004; Blain et al. 2004a). Similarly, our radio preselection means that we are missing a small fraction of colder SMGs without radio counterparts, which may contribute to the number density of $z \sim 2.5$ galaxies with $L_{\rm FIR} > 10^{12}\ L_\odot$ (Ivison et al. 2005). We anticipate that the deep *Spitzer*

observations of all these high-redshift galaxy populations will shed additional light on this complex question.

4.3. *The Rest-Frame UV-derived $L_{\rm FIR}$ of SMGs*

By far the best-studied population of high-redshift star-forming galaxies is composed of those identified through their rest-frame UV emission (Steidel et al. 1999, 2004). These galaxies have provided unique insights into the evolution of the star formation density in the universe and the corresponding formation of normal galaxies (Madau et al. 1996). A key question for SMGs is to understand how they fit into the framework defined by the UV populations—in particular, how well does the recipe for deriving SFRs for UV-selected galaxies work on this rest-frame FIR-selected population?

We can use our multicolor optical data for a subset of the SMGs to investigate their rest-frame UV properties and derive SFRs in an analogous manner to that applied to LBGs. This analysis relies on estimating the luminosities and spectral slopes at a wavelength around 1500 Å in the rest frame. For galaxy populations at $z \sim 2$–3, this can be achieved using *B*- and *R*-band photometry for the HDF sources and using *g*- and *R*-band photometry for the SSA22 and Westphal-14 sources.

As described in § 2, we measured *BR*-band photometry for all SMGs in our sample. Since UV-derived luminosities and the corrections for dust extinction are highly susceptible to photometric errors (Adelberger & Steidel 2000), we need to isolate a sample of SMGs with well-measured photometry. Unfortunately, most SMGs at higher redshifts are faint, with the result that to obtain a reasonable sample we are required to use those galaxies for which the photometric errors are only <0.1 mag in both bands. We define the subsample that includes all 33 SMGs lying in the HDF, Westphal-14, and SSA22 fields with redshifts $z > 1.5$ to allow for accurate measurement of the dust-corrected UV luminosity (the same sample used in Fig. 5). We also consider the HDF subsample on its own (17 SMGs), since its large size and contiguous areal coverage make it statistically representative on its own. The sample has a median $R_{\rm AB} = 24.9$ and a 1 σ rms of 1.1 and a median photometric error of $dR_{\rm AB} = 0.04$. The dust-corrected luminosities are biased in a manner that is difficult to quantify. The optically faintest sources have very small UV luminosities, but they may in principle have very steep continuum slopes, with large implied dust correction factors (Adelberger & Steidel 2000). While we will calculate UV luminosities for all SMGs in this subsample, we identify those SMGs showing AGN spectra and conservatively exclude them from the average properties calculated below.

To estimate the SFR from the UV, we follow the prescriptions of Meurer et al. (1997) and Adelberger & Steidel (2000). The UV luminosities are first corrected for line blanketing in the Lyα forest and then corrected for dust extinction using the UV continuum slope derived from the $G - R$ color, corresponding to wavelengths between rest-frame 1000 and 2900 Å. The transformations from the measured $B - R$ to $g - R$ in the HDF field are described in § 3.4. We correct the $g - R$ color for the opacity of the Lyα forest according to the statistical prescription of Madau (1995). Values of $(g - R)_{\rm corr}$ ranging from 0.0 to 1.0 correspond to a UV spectral index $\beta = -2$ to +0.6, when the spectrum is approximated by a power law of the form $F_\lambda \propto \lambda^\beta$. The $(g - R)_{\rm corr}$ color is then mapped to a color excess, $E(B - V)$, from which the dust-corrected UV luminosities are derived. Our median $\beta = -1.5 \pm 0.8$, corresponds to $E(B - V) = 0.14 \pm 0.15$ for a Calzetti extinction law, very close to the distribution for LBGs presented in Adelberger & Steidel (2000), suggesting that the UV identifications of SMGs do not distinguish themselves from the general LBG population with significantly redder UV spectral slopes (see Smail et al. 2004).

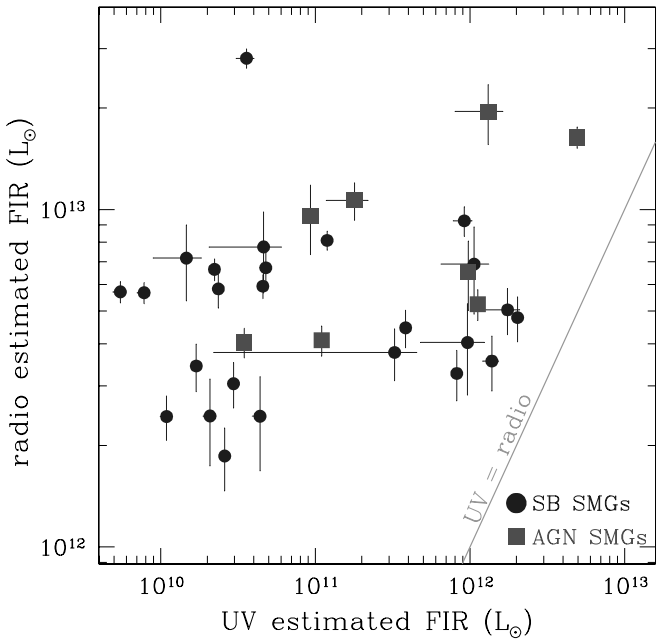

FIG. 11.—FIR luminosity of SMGs (used as a proxy for their SFRs) as measured from the radio and submillimeter flux density ratio, compared with the FIR luminosity estimated from the UV luminosity and spectral slope. The line is a simple equality, $L_{\rm FIR}({\rm radio}) = L_{\rm FIR}({\rm UV})$, the expected correlation if the dust-corrected UV luminosity is a reliable measure of the total SFR in these systems. Note the large offsets of most SMGs from this line. Error bars are derived from uncertainties on the radio, submillimeter, *B*- or *g*-, and *R*-band fluxes. SMGs showing obvious AGN spectra are shown by large squares. There are no upper limits, as we include only those SMGs in the HDF, Westphal-14hr, SSA22, and ELAIS-N2 fields that are detected in both the *B* and *R* bands.

The dust-corrected UV luminosity translates into an SFR, following Kennicutt (1998):

$$\mathrm{SFR}(M_\odot\ \mathrm{yr}^{-1}) = 1.4 \times 10^{-28}\ L_{1500}(\mathrm{ergs}^{-1}\ \mathrm{Hz}^{-1}),$$

where the relationship applies to galaxies with continuous star formation over timescales of 10^8 yr or longer. For younger stellar populations, the UV continuum luminosity continues to increase as the number of massive stars increases, which means that the above equation underestimates the SFR. Finally, to compare these estimates with those from the FIR, we simply convert our UV-derived SFR directly into a FIR luminosity (Kennicutt 1998).

From the dust-corrected UV, we predict a median FIR luminosity of $0.05^{+0.02}_{-0.04} \times 10^{12}\ L_\odot$; this compares with the submillimeter/radio measurement of $L_{\rm FIR} = 5.6^{+2.1}_{-1.6} \times 10^{12}\ L_\odot$. This corresponds to a median radio/submillimeter-to-UV ratio in the derived $L_{\rm FIR}$ of 120, with a quartile range of 24–187. We reiterate that the UV estimate has been *corrected* for dust extinction in the standard manner. The dust-corrected UV-estimated FIR luminosities are compared directly with the FIR luminosities measured from the radio/submillimeter in Figure 11. The relative offset between the two does not differ significantly if we use the more statistically reliable subsample from the HDF: $L_{\rm FIR,UV} = 4.28^{+1.51}_{-3.40} \times 10^{10}\ L_\odot$ versus $L_{\rm FIR,radio} = 5.79^{+1.96}_{-1.41} \times 10^{12}\ L_\odot$. In addition, we note that those sources in the HDF with the faintest apparent *R*-band magnitudes do not have significantly different UV-inferred $L_{\rm FIR}$ from those with brighter *R* magnitudes.

As suggested above this procedure of estimating the FIR luminosity from the UV continuum slope is meaningless for the

SMGs exhibiting strong AGN signatures in their spectra, since the UV continuum is not necessarily dominated by stellar emission, and so we have not included these AGN-classified SMGs in the median calculations given above. We use different symbols for the SMGs with AGN spectra in Figure 11 to identify them to the reader.

Since the FIR-radio luminosity relation is essentially linear, except at the faintest extreme (Condon 1992), the relation at high redshift would have to vary by a similar factor to our observed discrepancy ($\sim$100) for the luminosity estimates to be in accord. This is highly unlikely given the relatively well-understood physics of the relation (Condon 1992). However, direct measurements of the FIR-radio relation at high redshift are required to refute this possibility. (We can begin to rule out evolution of FIR-radio at the implied level of a factor of $\sim$100, based on the previous discussion in § 4.1; A. Kovacs et al. 2005, in preparation.)

Clearly the *dust-corrected* UV luminosity using the standard prescription rarely hints at the huge bolometric luminosities measured in the radio/submillimeter, underestimating the true luminosity by more than 2 orders of magnitude. Four of the SMGs *do* have UV-inferred luminosities within a factor of 3 of that observed in the radio/submillimeter. One of these shows hybrid SB/AGN characteristics and complicated multicomponent kinematics (SMM J163650.43+405734.5; Smail et al. 2003a). The other three are apparently starbursts that reveal the true magnitude of their bolometric luminosity in the UV.

The very large disparity we derive for the UV- and radio-estimated luminosities of UV-detected SMGs is apparently at odds with the conclusion of Reddy & Steidel (2004), who find that radio (and X-ray) estimates of the SFRs for $z \sim 2$ BX galaxies on average match the UV-derived SFRs, with an average dust correction factor of just 4.5. How do we reconcile this with our finding that SMGs have UV-inferred SFRs that underpredict the radio-measured SFR by a factor of 120 on average? One possible contributing factor is that there may be a wide range in dust obscuration in the high-redshift galaxy population. Chapman et al. (2004) used MERLIN radio images and *HST* UV images of SMGs at $\sim$0.″3 resolution to study the differential emission between the two wavelengths. They demonstrated that the radio emission (and by implication submillimeter emission) is always more compact than the UV as traced by *HST* imagery. In addition, they found that the radio highlights regions of low UV emission as bolometrically luminous in $\sim$50% of the SMGs. An increasing proportion of very highly obscured activity may therefore be present in the more active systems. This has also been demonstrated through measurements of the nebular Hα emission line for our SMG sample (Swinbank et al. 2004). In this way the selection of flux-limited samples of galaxies in the rest-frame UV and FIR would give significantly different mean obscurations. This is equivalent to stating that the UV luminosities and spectral slopes are measurable for only the least-obscured regions of the galaxies and hence are not representative of the bulk of the emission in these galaxies. It is therefore not surprising that they indicate much lower bolometric emission.

We therefore conclude that although many SMGs can be detected and their redshifts estimated or measured in deep observations in the rest-frame UV, they cannot generally be identified as bolometrically luminous galaxies without the use of radio or submillimeter observations. There is a second, related important point to make before we proceed to discuss the evolutionary history of the luminosity density contributed by SMGs versus UV-selected galaxies over the lifetime of the universe. In light of the vast mismatch in the derived bolometric emission for this population we assume that the contribution of bright SMGs to the star formation density at high redshifts is not included in current UV estimates (e.g., Madau et al. 1996; Steidel et al. 1999)—and so we need to derive the contribution from the highly obscured population independently and sum this with that from the UV to derive the total.

4.4. *Luminosity and Star Formation Histories*

Using the bolometric luminosities measured above for the SMGs, we calculate the following bolometric luminosity densities in redshift bins from our survey: $\rho_L(10^7\ \mathrm{Mpc}^{-3}) = 2.0 \pm 2.3$, $8.1^{+4.9}_{-3.2}$, and $3.4^{+4.6}_{-2.5}$ for redshift intervals of $z = 0.5$–1.2, 1.8–2.6, and 2.6–3.5, respectively. These luminosity densities are calculated for the entire radio-identified SMG population and corrected for spectroscopic completeness in the following way. For the 26% of radio SMGs for which we did not obtain redshifts, we corrected the clear deficit of sources in the redshift range $z = 1.2$–1.8, resulting in a smooth distribution matching our normalized model (Fig. 4). The remainder of the incompleteness (17%) was distributed uniformly over the entire $N(z)$ uncovered by our robust redshift sample. Our justification for this procedure is twofold. First, the $S_{850\ \mu\mathrm{m}}/S_{1.4\ \mathrm{GHz}}$ properties of sources with robust redshifts are indistinguishable from those for which we did not obtain redshifts, suggesting a similar range in T_d and z. Second, the *UBR* colors of these two samples are similar, although with large uncertainties because many of the spectroscopic failures are typically very faint, and are consistent with colors of $z \sim 2$ star-forming galaxies (Steidel et al. 2004) (see § 3.4).

In order to justify translating these luminosity densities into star formation rate densities (SFRDs), we must first clearly identify the signs of AGN activity in the individual galaxies and then remove any contribution to the luminosities of these galaxies from the AGN, either in the form of a direct contribution to the radio emission or through heating of dust by the AGN.

We begin by assessing the possible AGN contribution in individual SMGs from their UV spectral properties. Three SMGs are identified with QSOs in our radio-identified sample (SMM J123716.01+620323.3, J131215.27+423900.9, and J131222.35+423814.1): these are the only objects for which the optical luminosity is a nonnegligible fraction of the bolometric luminosity. These sources have comparable optical and FIR luminosities and space densities to submillimeter-detected QSOs at $z > 2$ (Omont et al. 2001, 2003; Carilli et al. 2001). The fraction of optically bright QSOs in the SMG population could actually be slightly higher, since $\sim$20% of our SMGs were preselected with optically faint magnitudes. This implies that only $\sim$4% (3/80, as a fraction of the total radio SMG sample observed spectroscopically, which were not pre-selected as optically faint) of optically bright AGNs have L_{FIR} emission with comparable luminosity to that seen in the optical waveband (since our survey would have uncovered all the QSOs emitting strongly in the radio/submillimeter). This fraction of radio SMGs are therefore removed from consideration in determining the luminosity density evolution.

There are several strong indications that star formation dominates the luminosity of the majority of the 98 radio SMGs in our sample. As discussed in § 3.3, 30% of the objects in our sample with the brightest UV continua exhibit stellar and interstellar absorption lines, implying that their continua are dominated by young, massive stars and not the nonthermal power-law spectrum of an AGN. Another 25% of our sample have UV continua that are too faint to detect absorption features but remain consistent with starbursts, while a further 25% do not reveal enough features to even identify a redshift. These statistics

suggest that ~80% of radio SMGs do not harbor a partially or unobscured, luminous AGN.

The presence of an obscured AGN is much more difficult to determine from the rest-frame UV spectra, and instead we have to turn to multiwavelength surveys of samples of SMGs. High spatial resolution radio observations of SMGs are one route for determining the morphology of their radio (and by implication FIR) emission and hence search for the presence of a strong AGN contribution to the FIR (identified as a radio point source). Such studies reveal extended morphologies on scales $>1''$ in 65% of cases (8/12 galaxies in Chapman et al. 2004). These observations suggest that AGN do not dominate the FIR emission of most SMGs, as star formation is the most likely route to produce spatially extended FIR/radio emission. Several of the galaxies with spatially extended radio emission show AGN emission lines in their rest-frame UV spectra, underlining the fact that intense starbursts are likely to be energetically important, even in the presence of AGNs.

A second route to search for obscured AGNs is to employ observations in the X-ray waveband. The proportion of the submillimeter population detected in deep *Chandra* and *XMM-Newton* X-ray surveys, which are sensitive to even strongly dust-obscured AGNs (Ivison et al. 2002; Barger et al. 2002; Almaini et al. 2003; Alexander et al. 2002, 2005a), at flux densities significantly greater than expected from star formation alone is at most 30%. X-ray spectral analysis reveals that most of the SMGs are not Compton-thick sources with QSO-like luminosities and instead suggest that the AGNs in SMGs have modest X-ray luminosities (Alexander et al. 2005a).

Two more recently pursued routes to search for the presence of an AGN within an SMG are to use near-infrared spectroscopy and mid-infrared imaging. Swinbank et al. (2004) report on near-infrared spectroscopy of 24 SMGs from our sample. Of the 15 SMGs classified as star forming from their UV spectra, the emission-line properties (line widths and [N II]/Hα flux ratios) in the rest-frame optical support this classification for 60%, a further 20% have intermediate classifications (Hα line widths of 500–1000 km s^{-1}) and only 20% are clear cut AGNs based on their rest-frame optical spectra. This broadly supports our UV spectral classifications and implies that only ~30% of SMGs are likely to host luminous AGNs. A similar rate of identification of AGN-like SEDs (20%–30%) is found in recent *Spitzer* mid-infrared photometric studies of SMGs: 2/13 from the combined sample of Ivison et al. (2005) and Egami et al. (2004) and 2/7 for the radio-identified SMGs in Frayer et al. (2004).

We conclude, using a number of independent indicators, that around 20%–30% of SMGs show detectable signs of AGN activity. The broad agreement on this proportion among such a wide range of indicators gives us confidence that it represents a true limit to the extent of AGN activity in the population. We stress that this does not indicate that 30% of the FIR emission from these galaxies comes from AGNs. Even when an obvious and strong AGN is present in an SMG, there are signs that it does not dominate the bolometric emission (e.g., Frayer et al. 1998). The AGN contribution to the luminosity of the whole SMG population may be as low as 10% (Alexander et al. 2005a). Using the results that $\lesssim$30% of SMGs have properties indicative of an AGN, we will conservatively assume that 70% of the FIR luminosity is derived from star formation in the total SMG population.

The luminosity densities we estimated earlier can now be translated into SFRDs by scaling them down by 30% to account for a maximal AGN-contribution and then using the standard calibration of $(1.9 \pm 0.3) \times 10^9\ L_\odot\ (M_\odot\ \mathrm{yr}^{-1})^{-1}$ (Kennicutt 1998). We plot the resulting SFRDs in Figure 12.

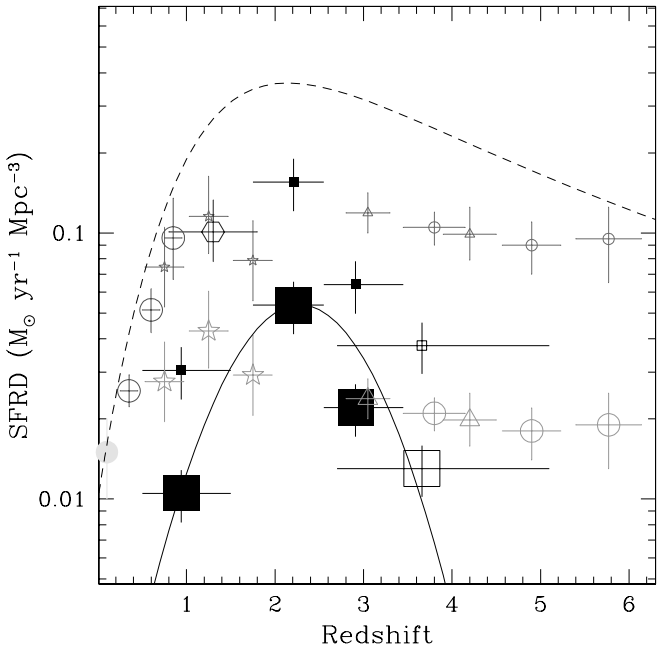

FIG. 12.—Evolution of the energy density (parametrized by SFRD) in the universe with epoch. Our new submillimeter measurements (*large squares*, shown at the median value for each redshift bin) are compared with the published estimates from optical/UV surveys and radio/IR tracers of the star formation density. The open square indicates the SMGs without radio identification, at the median redshift derived from our modeling of Fig. 4. The smaller symbols for the optical estimates indicate dust-corrected estimates. A Gaussian fit is shown for the four submillimeter galaxy points, tracing an evolution comparable to luminous radio-selected quasars (Shaver et al. 1998). For the submillimeter sources, the smaller points show a simple redshift-independent correction to the luminosity density to match the submillimeter extragalactic background down to 1 mJy. The dashed line is the best fit for a simple parametric model constrained by the counts of sources in the FIR/submillimeter and the spectrum of the extragalactic background (Blain et al. 2002). Other UV-, mid-IR–, and radio-derived points are from Giavalisco et al. (2004; highest z, *circles*), Steidel et al. (1999; $z = 3$–4, *triangles*), Connolly et al. (1997; $z = 1$–2, *stars*), Yan et al. (1999; $z = 1.3$, *hexagon*), Flores et al. (1999; $z = 0.3$–1, *circles*), Yun et al. (2001; low z, *solid circle*).

An additional point has been plotted on Figure 12 to represent the ~35% of the total SMG population that is not detected in our radio maps. The redshifts of these objects are assumed to follow the radio-undetected fraction from our $N(z)$-normalized model (Fig. 4), implying a significant overlap with the redshift range probed by our radio SMG sample. The redshift range we show for the radio-undetected sample extends to $z = 5.1$, at which point fewer than one SMG would lie in a total SMG sample of 151 galaxies (our targeted 98 radio SMGs, plus an extra 35% undetected in the radio). This *uniform population* model is the most intuitive representation of the radio-unidentified SMGs, but we stress that it is based purely on a model, and it is possible that the radio-undetected galaxies have a very different distribution that the one we predict, extending to higher redshifts, or even a bimodal distribution compared with our well-characterized radio SMGs.

We can now estimate the evolution of the SFRD for all SMGs brighter than ~5 mJy at 850 μm. A solid curve is plotted in Figure 12, representing a Gaussian fit to the four SMG points (after redistributing the objects in the high-redshift bins into two nonoverlapping bins in redshift). The fit is

$$\mathrm{SFRD} = 1.26 \exp\left[-(z - 2.18)^2/\sigma^2\right],$$

with $\sigma = 1.30$. This evolutionary behavior is quite similar to that inferred for the luminosity density of quasars (e.g., Boyle et al. 2000; see Fig. 5).

We also plot in Figure 12 the SFRD estimated from a number of UV-selected galaxy surveys at $z = 1$–6 (Connolly et al. 1997; Steidel et al. 1999; Giavalisco et al. 2004) and low-redshift ($z < 1$) radio and mid-IR observations (Yun et al. 2001; Flores et al. 1999). A dust-correction of a factor of 5 for the $z \sim 3$ LBG population (Pettini et al. 2001) has been applied to the high-redshift UV-selected populations to give their dust-corrected estimates. Recent analysis of the SFRD evolution via C II* λ1335.7 in damped Lyα absorbers suggests a total SFRD comparable to the dust-corrected UV estimates (Wolfe et al. 2003a, 2003b).

This analysis allows us to bring together the various high-redshift populations. Figure 12 highlights the relative importance of different classes of high-redshift, star-forming galaxies, which is critical for a full understanding their relative importance in galaxy evolution. We see that although the bright, radio-detected SMGs presented here represent only 20% of the 850 μm background, the estimated star formation density at $z = 2$–3 is within a factor of 2 of that inferred from rest-frame UV observations (Steidel et al. 1999; Adelberger & Steidel 2000). Including a contribution from the more numerous, less luminous SMGs with 850 μm fluxes below $\sim$5 mJy would result in their SFRD matching or even exceeding that seen in the UV. Moreover, as we argued in the previous section, the SFRD contribution of this population is effectively missed by UV-selected surveys, and hence we must *sum* the bright SMG and UV estimates to determine the *total* SFRD.

We also need to account for the large fraction of the submillimeter galaxy population that is below our $\sim$5 mJy flux limit at 850 μm. We chose only to integrate down to 1 mJy, as this is the flux scale at which the estimated SFR of typical UV-selected galaxies becomes comparable to the FIR sources. There is a correction factor of $\sim$2.9 that is required for the submillimeter points to account for the SMGs integrated down to 1 mJy, comprising $\sim$60% of the extragalactic background in the submillimeter waveband (Smail et al. 2002). We apply this correction to Figure 12, assuming that these fainter SMGs share the same redshift distribution as the brighter SMGs whose distribution is explicitly measured in this paper. The SFRD measurements corrected in this manner would suggest that SMGs are the dominant site of star formation activity in the universe at $z \sim 2$–3. However, the discussion below suggests that our assumption of a similarity between the redshift distributions of bright and faint SMGs is likely to fail, even by flux densities of $S_{850} \sim 1$ mJy (see also C. G. Lacey et al. 2005, in preparation).

A second important point to draw from Figure 12 concerns the relative evolution of the UV- and submillimeter-selected populations. Our redshifts show that SMGs are coeval and energetically comparable in a volume-average sense with the population of UV-bright, star-forming galaxies detected at $z \sim 2$–3 (Steidel et al. 1999). However, the SMGs with $S_{850\,\mu\mathrm{m}} > 5$ mJy and UV-selected galaxies (which have a median 850 μm flux of $\lesssim$0.5 mJy; Adelberger & Steidel 2000; Reddy & Steidel 2004) clearly do not evolve in the same manner. SMGs appear to evolve more strongly than the UV-selected population out to $z \sim 2$ (C03) and indeed seem to behave in a manner very similar to luminous quasars and X-ray–selected AGNs, whose luminosity density peaks at $z \sim 2.3$ (Boyle et al. 2000; Croom et al. 2004; Silverman et al. 2005). As Figure 12 makes clear, this is in stark contrast with the individually less luminous, UV-selected galaxies whose comoving luminosity density is approximately constant out to at least $z \sim 5$ (Lehnert & Bremer 2003; Giavalisco et al. 2004). This suggests that the properties of the bright submillimeter population is more closely linked with the formation and evolution of the galaxies or galactic halos that host QSOs than the more typical, modestly star-forming galaxies identified from their rest-frame UV emission. Nevertheless, there is likely to be an intermediate-luminosity regime in which the UV- and submillimeter-selected populations overlap significantly and therefore in which their evolution becomes similar—we propose that this likely occurs at submillijansky levels.

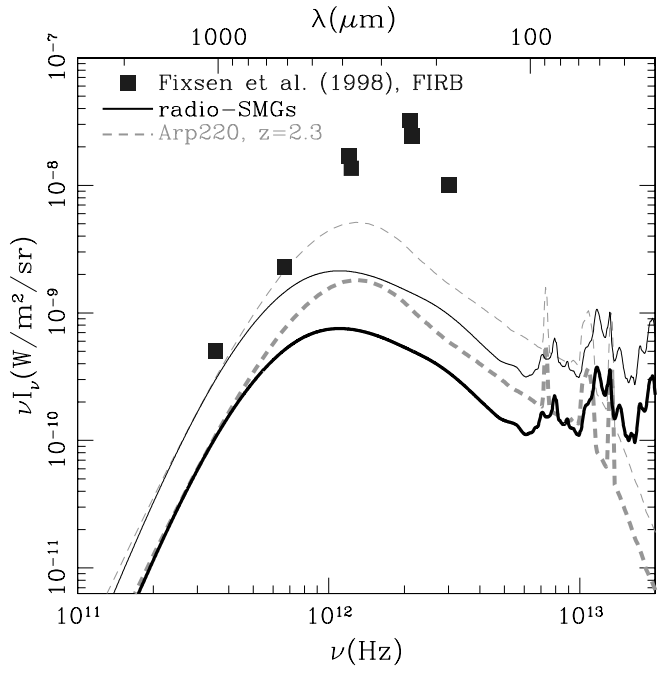

FIG. 13.—Measurements of the FIR background from Fixsen et al. (1998) and the contribution per unit wavelength of spectroscopically identified SMGs (*heavy solid line*). A curve representing Arp 220 at $z = 2.3$ is shown normalized to our total 850 μm flux (*heavy dashed line*). We also show these two models, but corrected to account for the 850 μm background as resolved by submillimeter observations down to 1 mJy (Blain et al. 1999a, 1999b; Cowie et al. 2002), as thin curves.

4.5. *Contributions to the FIR Background*

Using our the long-wavelength SEDs that we fitted to the submillimeter/radio observations of the SMGs, we can calculate their contribution to the extragalactic background at other wavelengths in the FIR. The measured and the contribution per unit wavelength from our SMGs with redshifts and well-fitted SEDs are shown in Figure 13. At 850 μm this is simply the sum of the flux measurements for our SMGs normalized by the effective survey area (assuming a radio-detected fraction of 65%). At all shorter wavelengths, the curve represents the sum of the best-fit SEDs, examples of which were shown in Figure 8. We see that the SMG sample we are studying contributes around 20% of the background at >600 μm and a diminishing fraction at shorter wavelengths.

To provide a simple baseline comparison we also illustrate the contributions to the FIRB if all of the SMGs lie at $z = 2.3$ (the median redshift of our model-corrected spectroscopic sample) and have SEDs matching that of Arp 220, again normalized to our total 850 μm flux. Note that the actual peak of the background due to the SMGs is significantly broadened by the

dispersion in their redshifts and dust temperature, compared with a single $T_d \sim 45$ K–like Arp 220 SED at $z = 2.3$.

The contribution of SMGs to the peak of the FIRB varies on a galaxy-by-galaxy basis by a factor of $\sim$10. Galaxies with hotter characteristic dust temperatures contribute more, but because they typically lie at higher redshifts in our submillimeter-selected sample, their contribution is scaled down. Splitting our sample into high- and low-redshift bins, we assess the relative contribution to the emission around the peak of the FIRB at $\sim$200 μm as a function of redshift. SMGs at $z = 2.8 \pm 0.3$ contribute 3 times less to the FIRB than SMGs at $z = 2.2 \pm 0.3$. This implies that the increase in characteristic T_d with redshift is not fast enough to counteract the diminution of rest-frame 200 μm flux from the *K*-correction. If we include plausibly identified SMGs without radio detections (Ivison et al. 2005), which are predicted to have colder dust temperatures, we find that their contribution to the FIRB is much smaller (by a factor $\sim$5) compared with the warmer T_d radio SMGs. Moreover, the radio-unidentified SMGs are spread throughout both redshift bins, and they do not substantially affect the relative FIRB contributions as a function of redshift.

We can also estimate the contribution of the bulk of the submillimeter galaxy population to the FIRB by applying a correction factor (times 2.9) to our composite SMG template to include galaxies down to 1 mJy, comprising $\sim$60% of the Fixsen et al. (1998) 850 μm background.

This extrapolation suggests that galaxies selected at 850 μm are significant contributors (responsible for $\gtrsim$30% of the total emission) to the FIRB at wavelengths of $\gtrsim$400 μm, assuming that modest extrapolations up the luminosity function are composed of galaxies similar in characteristics to those SMGs in our sample. However, the >1 mJy SMG population probably contributes no more than 6% of the emission at the peak of the FIRB at $\sim$200 μm, which is dominated by lower redshift and/or hotter populations. For sources fainter than 1 mJy, there is likely to be a wider distribution of redshifts, and predictions based on our bright submillimeter sample are much more uncertain.

The procedure we used in the calculation above assumes that submillimeter sources with flux densities fainter than our sample have a similar redshift distribution and range of SEDs/dust temperatures. There is some evidence for this down to 1 mJy from cluster lensed SMGs (e.g., Smail et al. 2002; Borys et al. 2004; Kneib et al. 2004). We discussed in the previous subsection why this may not be a good approximation fainter than 1 mJy: UV-selected galaxies appear to have a very different evolution history from SMGs, and the UV galaxies are likely to contribute a substantial fraction of the submillimeter background at $\sim$0.1 mJy flux densities. The corrected distribution should therefore be assessed critically. Specifically, if fainter sources begin to evolve more like UV-selected galaxies, with less of a peak at $z \sim 2.5$, then these higher redshift and less luminous sources will have a progressively smaller contribution to the FIRB near 200 μm.

4.6. *Mid-/Far-IR Spitzer Fluxes and Spectral Diagnostics*

The *Spitzer Space Telescope* marks a new era in infrared astronomy, pushing significantly deeper than past space infrared missions. A pressing question is therefore the overlap of the SMGs with the faint *Spitzer* population. By assuming the locally calibrated SEDs of Dale & Helou (2002), we demonstrate that our observed factor of 2 range in submillimeter flux translates into greater than 2 orders of magnitude in 24 μm flux, with the faintest galaxies having predicted fluxes of only 10 μJy (see Fig. 8). Prior to obtaining redshifts for SMGs, it was impossible to realistically assess the required sensitivities for IR follow-up with *Spitzer*. Several authors have already suggested that the detection rate of SMGs by *Spitzer* at 3.6–24 μm is very high (Frayer et al. 2004; Ivison et al. 2005; Egami et al. 2004), with flux densities roughly in accord with our predictions in Figure 8.

Mid-IR spectral surveys with *ISO* (Lutz et al. 1999; Tran et al. 2001) demonstrated that this wavelength regime is a powerful tool to classify the energetics of galaxies in an independent manner from conventional optical classification techniques (e.g., Swinbank et al. 2004). The main advantage of the mid-IR is that it probes the physical conditions in the more obscured regions closer in to the optically thick, dust-enshrouded nuclei and molecular cloud regions of the galaxies at which the bulk of the FIR emission arises (Sturm et al. 2000, 2002; Verma et al. 2003; Spoon et al. 2004). Key emission features include those from polycyclic aromatic hydrocarbon (PAH) at 6–18 μm, high-excitation Ne emission lines and the broad silicate absorption feature. It has been suggested that some of these features are diagnostic of the relative balance of dust heating by AGNs and star formation.

Spitzer spectroscopy of SMGs to determine mid-IR properties will be important for disentangling the physical conditions in the most active regions within these highly obscured galaxies. The Dale & Helou (2002) spectral templates include PAH features, Ne emission, and the broad silicate absorption feature, all estimated as a function of luminosity and temperature on the basis of local correlations. Our template fits to the SMGs with redshifts therefore allow predictions of their mid-IR spectral properties (Figs. 8 and 13), indicating that low-resolution *Spitzer* spectroscopy should yield line detections for the majority of the SMGs in our sample. Indeed, stacking *Spitzer*-IRS spectra for similar classes of SMGs should yield sufficient S/N to study the shape of the PAH feature and probe the chemical evolution of silicates (e.g., Honda et al. 2004).

However, it is possible that the physical properties in high-z ULIRGs (such as the gas fraction, metallicity, star formation extent, and SFR) may differ from these local systems. For example, a comparison of the UV and long-wavelength morphologies of SMGs indicates that their star formation is more spatially extended than that in the local population of ULIRGs (Chapman et al. 2004), likely resulting in differences in the physical conditions experienced by dust grains (Lu et al. 2003). Mid-IR spectroscopy of SMGs may be able to test this claim and provide new insights into the physics of SMGs.

4.7. *The Duty Cycle of SMGs*

Having discussed the observational and inferred properties of our SMG sample, we wish to finish by discussing their evolutionary connections to other populations at high and low redshifts. In order to connect the SMG population to a likely population of descendents, we must estimate what the duty cycle for SMGs might be. Our greatest uncertainty in this calculation is the duration of the submillimeter-luminous event. Smail et al. (2003a, 2004) estimated the past duration of the starburst events using both fits to the UV spectra with the Starburst99 synthetic templates (Leitherer et al. 1999) and simple model fits to the optical and near-IR photometry. They conclude that the starbursts have been ongoing for $\sim$10–100 Myr. Using the gas masses from the CO observations compiled for a small sample of SMGs by Neri et al. (2003), we can infer that there is enough molecular gas present in a typical SMG to continue the starbursts at their present rate for at most another $\lesssim$100 Myr and perhaps considerably less. Thus, the total duration of these submillimeter-luminous events might be $\sim$100 Myr.

The length of the starburst is likely to be regulated by the enormous superwind outflows that are expected to be driven in SMGs; Greve et al. (2005) and Smail et al. (2003a, 2004) demonstrated offsets between Lyα and molecular CO or Hα as large as 1000 km s^{-1}, implying outflows of large velocity. The SMGs are the most luminous galaxies in the universe and as such are expected to drive some of the largest superwinds, which, if the mass ejected is proportional to the SFR (Heckman 2002), would produce typical outflows of 1000 $M_{\odot}$ yr^{-1}. Simple scaling arguments suggest that the kinetic energy put into SMG winds (and hence the local environment) would be $\sim$10 times that of LBGs, which are already known to show evidence for strong outflows (Adelberger & Steidel 2003). Given the potential power of this feedback mechanism, we must treat our estimated submillimeter-luminous timescale as an upper limit, since the outflows and associated turbulence could easily turn the starburst off in a shorter time period.

The radio-identified SMG redshift distribution was well fitted by a Gaussian with a central redshift of 2.2 and $\sigma_z \sim 1.2$ (accounting for incompleteness in the spectroscopic desert). Modeling of the full SMG redshift distribution suggests $\sigma_z \sim 1.3$, although this is clearly dependent on the model adopted. Focusing just on the radio-identified SMGs, these populate a period of about 1 Gyr. Dividing the submillimeter redshift distribution by the submillimeter-luminous timescale of 100 Myr suggests a duty cycle of 10. In other words, there is an underlying population of galaxies 10 times as numerous as the SMGs that correspond to the immediate progenitors and descendents of the SMG phenomenon. This parent population would have a volume density at $z = 1$–3 of $\sim 10^{-4}$ Mpc^{-3} and would be expected to have the similar clustering properties to the SMG events themselves ($r_0 \sim 7\ h^{-1}$ Mpc; Blain et al. 2004b). One possible identification of the descendents of the SMG population comes from the discovery of luminous, near-IR galaxies at $z \sim 2$ with apparent stellar ages of 1–2.5 Gyr, stellar masses of $1\text{–}5 \times 10^{11}\ M_{\odot}$ and a space density a factor of several times higher than SMGs (van Dokkum et al. 2003, 2004; Franx et al. 2003; Glazebrook et al. 2004).

To understand the evolutionary connections of the SMGs with other galaxy populations at similar redshifts, it is crucial to measure the SMG clustering properties. Surprisingly, even with our small sample, we are already in a strong position to characterize the clustering. We note in Table 2 that SMGs often come in pairs or larger associations to about 1200 km s^{-1}, with approximately one in five SMGs in our sample lying in such associations. This can be quantified into an estimate of the clustering strength (Blain et al. 2004b), suggesting a correlation amplitude comparable to low-redshift EROs (e.g., Daddi et al. 2001; McCarthy et al. 2001). The SMG associations seem to point to global overdensities in the galaxy populations, typified by the $z = 3.1$ protocluster in the SSSA22 field (Steidel et al. 1999), where three SMGs lie at $z = 3.1$. The five SMGs at $z = 2.0$ in the HDF suggest that we have likely identified another overdensity of a similar scale to the SSSA22 protocluster.

The clustering scale of 2dF QSOs is similar to that of SMGs within errors (QSOs: $r_0 \sim 5$ Mpc, Croom et al. 2002; SMGs: $r_0 \sim 7$ Mpc, Blain et al. 2004b), and as we have noted repeatedly in this study, the redshift distributions of both populations are very similar. However, the volume densities of bright QSOs and SMGs do not match; the SMGs outnumber QSOs by a factor of $\sim$5–10 (C03). The SMGs and QSOs can be viewed as different phases of the same population if the timescales compensate for this discrepancy. Martini & Weinberg (2001) suggest that QSOs endure for $\sim$40 Myr, requiring that SMGs be active for $\sim$200–400 Myr, not too discrepant from our adopted SMG timescale of 100 Myr estimated above. Another possibility is that the QSO may often represent a phase in the active lifetime of a subset of SMGs, which depends on environmental conditions that facilitate the funneling of material from the extended SMG starburst to the growing central engine.

It is worth seriously considering the possibility of an interrelation between the SMG and QSO phenomena. The local *Magorrian* relation (Magorrian et al. 1998) between black hole mass and stellar bulge mass suggests that super-massive black holes (SMBHs) must be growing at a rate roughly proportional to the stars. The SMGs appear to be prodigiously forming stars, with the modest X-ray luminosities of SMGs suggesting either low rates of accretion onto SMBHs and/or moderate SMBH masses (Alexander et al. 2005a). Both of these possibilities suggest that substantial SMBH growth is needed to evolve onto a Magorrian relation. A logical conclusion is that the SMGs are indeed an early phase in the evolution of a massive galaxy, forming many stars quickly over $\sim$10 kpc spatial scales, as shown by the extended radio emission tracing UV structures (Chapman et al. 2004). As the merger proceeds, the growing SMBH begins to accrete material more quickly as instabilities drive material to more concentrated configurations. The SMBH thus grows ever more rapidly, on a timescale that is delayed from that of the initial starburst (see also Archibald et al. 2002), eventually blowing channels through the dust and becoming visible as a QSO. Indeed, Page et al. (2001) and Stevens et al. (2004) measured significant submillimeter emission from X-ray self-absorbed QSOs, suggesting that an intermediate stage between SMGs and QSOs is being directly observed. This is also consistent with the 3/80 QSO detection rate (4%) for our unbiased SMG sample, if it is assumed that all submillimeter-detected QSOs are X-ray absorbed (Stevens et al. 2004). Under this scenario, the proportion of X-ray–absorbed QSOs is one-sixth of the entire QSO population (Stevens et al. 2004), and hence the ratio of QSO to SMG lifetimes should be 18/80, or $\sim$0.23, consistent with the volume densities described above.

Most likely, the relationship between SMGs and other galaxy populations spans a range of scenarios and evolutionary histories, and more comprehensive models are required to understand and further test the evolution of SMGs.

5. CONCLUSIONS

We assembled a detailed account of the properties of the radio-identified SMGs. Spectroscopic redshifts have been obtained for 73 radio SMGs from deep optical spectroscopy of 98 targets attempted, for a success rate of 74%. The redshift distribution of SMGs is now well constrained—showing a pronounced peak at $z \sim 2.2$ for our radio-selected sample and a predicted median of $z \sim 2.3$ for a purely submillimeter-flux–limited sample, similar in form to distribution seen for radio-, optical-, and X-ray–selected QSOs. We also demonstrate that the simple radio/submillimeter redshift estimator, which has been used extensively in the literature to attempt constraint the redshift distribution of SMGs, is not reliable for individual SMG redshifts ($\Delta z \sim 1$). For the SMGs that are detectable with good S/N ($R < 26$) in deep ground-based images, photometric redshifts in the *UBRIK* bands appear to provide a more accurate constraint on the true redshifts of individual SMGs. We find that the radio SMGs for which we failed to obtain robust spectroscopic redshifts have similar $(U - g)/(g - R)$ colors to those with robust redshifts, and we conclude that the entire radio SMG population is likely to have a similar distribution to the spectroscopic redshift distribution presented here. We have also discussed the

likely redshifts of SMGs without radio identifications to fill in more details of the entire SMG population brighter than 5 mJy at 850 μm.

We measure dust temperatures and bolometric luminosities for SMGs by exploiting our precisely known redshifts and assuming the local FIR-radio correlation. The SED variation in our SMGs likely arises from a dispersion in dust temperature, but it could also arise from a broader scatter in the FIR-radio correlation than observed locally. If the SED variation were caused entirely by variations in the FIR-radio correlation, then the FIR-radio scatter would have to increase from the 0.2 dex observed locally to $\sim$0.8 dex. We view this as unlikely and so attribute most of the range in SED properties for the SMGs to differences in characteristic dust temperature.

We construct a bolometric luminosity function and compare with local *IRAS* galaxies, as well as estimates for UV-selected galaxies at $z \sim 2$–3. We predict the expected FIR luminosities of the SMG population on the basis of their UV luminosities and continuum slope, using the standard prescription for this conversion for UV-selected populations. We find that the true bolometric luminosity of an SMG is typically underestimated by $\sim$100 when extrapolated from their rest-frame UV properties. We therefore conclude that observations at radio/submillimeter wavelengths are essential to distinguish which $z \sim 2$–3 galaxies have the huge luminosities characteristic of SMGs.

We assess the SFRD evolution of SMGs, both from our observed $\sim$5 mJy SMG sample and from a modest extrapolation of our sample properties down to 1 mJy. Our results highlight the very different evolution of SMGs over UV-selected galaxies (noting the close similarity in evolution between SMGs and QSOs). This suggests that the properties of the bright submillimeter population are more closely linked with the formation and evolution of the galaxies or galactic halos that host QSOs than the more typical, modestly star-forming galaxies identified from their rest-frame UV emission. We emphasize that UV-measurements of the SMGs do not typically reveal the enormous bolometric luminosities present, and the SMGs and dust-corrected UV-selected galaxies in the SFRD diagram should be summed together to obtain a complete census of the SFRD evolution in the universe.

The SMG sample we are studying contributes around 20% of the background at >600 μm and a diminishing fraction at shorter wavelengths. The contribution of SMGs to the FIRB at $\sim$200 μm can be predicted by fitting dusty SED templates to the radio and submillimeter fluxes at the measured redshifts. This prediction is considerably less than expected from assuming an Arp 220–like SED, since the SMGs have cooler characteristic dust temperatures than Arp 220. The *Spitzer Space Telescope* is likely to provide important diagnostics of the highly obscured central regions of the SMGs through mid-IR imaging and spectroscopy.

We are rapidly approaching the point of being able to put all the evidence about properties of SMGs together. The spectroscopic redshifts allow us to study aspects of the SMG population that cannot be addressed using photometric redshift estimators. Astrophysical properties of the SMGs are diagnosed through the rest-frame UV and optical spectra themselves, probing, for example, the excitation conditions, metallicities, and wind outflows (Swinbank et al. 2004; I. Smail 2005, in preparation). The clustering of the SMGs is clearly a pressing question, and, surprisingly, even with our small sample we are already in a strong position to characterize the clustering through the redshift distribution, finding a correlation length $r_0 \sim 7\ h^{-1}$ Mpc (Blain et al. 2004b). The impact of SMGs on their environments and the intergalactic medium can be studied directly using background QSOs in the same fields (S. Chapman 2005, in preparation). With precise redshifts, X-ray spectral analysis in deep *Chandra* exposures is possible through the stacking of subgroups of SMGs with similar X-ray properties, yielding significant Fe II emission line detections and characterization of the X-ray spectral shape (Alexander et al. 2005b).

We conclude that with the availability of precise redshifts for large samples of FIR luminous galaxies, these populations can now be used to trace the evolution of the most luminous galaxies in the universe. A focus of our future work will be to identify the influence of this population on their environments.

We thank the referee, Paul van der Werf, for a thoughtful reading of the manuscript. S. C. C. acknowledges support from NASA through grants GO-9174 and GO-9856. A. W. B. acknowledges support from NSF grant AST 02-05937, from the Research Corporation, and from the Alfred P. Sloan Foundation. I. R. S. acknowledges support from a Royal Society URF. We thank Kurt Adelberger for kindly providing his suite of LRIS reduction scripts and instruction in their use. We would like to thank the following people for helpful discussions: C. Steidel, K. Adelberger, A. Shapley, N. Reddy, and C. Borys. The authors wish to recognize and acknowledge the very significant cultural role and reverence that the summit of Mauna Kea has always had within the indigenous Hawaiian community. We are most fortunate to have the opportunity to conduct observations from this mountain.

REFERENCES

Adelberger, K., & Steidel, C. 2000, ApJ, 544, 218
———. 2003, ApJ, 584, 45
Alexander, D., Smail, I., Bauer, F., Chapman, S., Blain, A., & Ivison, R. 2005a, ApJ, submitted
Alexander, D., Vignali, C., Bauer, F. E., Brandt, W. N., Hornschemeier, A. E., Garmire, G. P., & Schneider, D. P. 2002, AJ, 123, 1149
Alexander, D., et al. 2005b, Nature, in press
Almaini, O., et al. 2003, MNRAS, 338, 303
Archibald, E., et al. 2002, MNRAS, 336, 353
Aretxaga, I., et al. 2003, MNRAS, 342, 759
———. 2004, MNRAS, in press
Avni, Y., & Bachall, J. N. 1980, ApJ, 235, 694
Barger, A. J., Cowie, L. L., Mushotzky, R. F., & Richards, E. A. 2001a, AJ, 121, 662
Barger, A. J., Cowie, L. L., & Richards, E. A. 2000, AJ, 119, 2092
Barger, A. J., Cowie, L. L., & Sanders, D. B. 1999a, ApJ, 518, L5
Barger, A. J., Cowie, L. L., Smail, I., Ivison, R. J., Blain, A. W., & Kneib, J.-P. 1999b, AJ, 117, 2656
Barger, A. J., Cowie, L. L., Steffen, A. T., Hornschemeier, A. E., Brandt, W. N., & Garmire, G. P. 2001b, ApJ, 560, L23
Barger, A. J., et al. 1998, Nature, 394, 248
———. 2002, AJ, 124, 1839
———. 2003, AJ, 126, 632
Baugh, C. M., Lacey, C. G., Frenk, C. S., Granato, G. L., Silva, L., Bressan, A., Benson, A. J., & Cole, S. 2005, MNRAS, 356, 1191
Bertoldi, F., et al. 2000, A&A, 360, 92
Blain, A. 1999, MNRAS, 309, 955
Blain, A., Barnard, V., & Chapman, S. 2003, MNRAS, 338, 733
Blain, A., Chapman, S., Smail, I., & Ivison, R. 2004a, ApJ, 611, 725
———. 2004b, ApJ, 611, 52
Blain, A., Smail, I., Ivison, R. J., & Kneib, J.-P. 1999a, MNRAS, 302, 632
Blain, A., et al. 1999b, MNRAS, 309, 715
———. 2002, Phys. Rep., 369, 111
Bolzonella, M., Miralles, J.-M., & Pello, R. 2000, A&A, 363, 476
Borys, C., Chapman, S. C., Halpern, M., & Scott, D. 2003, MNRAS, 344, 385
Borys, C., et al. 2004, MNRAS, 355, 485

Boyle, B., et al. 2000, MNRAS, 317, 1014
Capak, P., et al. 2004, AJ, 127, 180
Carilli, C. L., & Yun, M. 1999, ApJ, 513, 13L (CY)
———. 2000, ApJ, 539, 1024
Carilli, C. L., et al. 2001, AJ, 122, 1679
Chapman, S. C., Blain, A., Ivison, R., & Smail, I. 2003a, Nature, 422, 695 (C03)
Chapman, S. C., Helou, G., Lewis, G., & Dale, D. 2003b, ApJ, 588, 186
Chapman, S. C., Lewis, G. F., Scott, D., Borys, C., & Richards, E. A. 2002a, ApJ, 570, 557
Chapman, S. C., Richards, E. A., Lewis, G. F., Wilson, G., & Barger, A. J. 2001a, ApJ, 551, L9
Chapman, S. C., Scott, D., Borys, C., & Fahlman, G. 2002b, MNRAS, 330, 92
Chapman, S. C., Smail, I., Ivison, R., & Blain, A. 2002c, MNRAS, 335, L17
Chapman, S. C., Smail, I., Ivison, R., Helou, G., Dale, D., & Lagache, G. 2002d, ApJ, 573, 66
Chapman, S. C., Smail, I., Windhorst, R., Muxlow, T., & Ivison, R. 2004, ApJ, 611, 732
Chapman, S. C., et al. 2000, MNRAS, 319, 318
———. 2001b, Deep Millimeter Surveys: Implications for Galaxy Formation and Evolution, ed. J. D. Lowenthal & D. H. Hughes (Singapore: World Scientific), 34
———. 2003c, ApJ, 585, 57
Chary, R., & Elbaz, D. 2001, ApJ, 556, 562
Condon, J. J. 1992, ARA&A, 30, 575
Connolly, A., et al. 1997, ApJ, 486, L11
Cowie, L. L., Barger, A. J., Fomalont, E., & Capak, P. 2004, ApJ, 603, L69
Cowie, L. L., Barger, A. J., & Kneib, J.-P. 2002, AJ, 123, 2197
Croom, S. M., Boyle, B. J., Loaring, N., Miller, L., Outram, P. J., Shanks, T., & Smith, R. J. 2002, MNRAS, 335, 459
Croom, S. M., Smith, R. J., Boyle, B. J., Shanks, T., Miller, L., Outram, P. J., & Loaring, N. S. 2004, MNRAS, 349, 1397
Cuillandre, J.-C., Luppino, G., Starr, B., & Isani, S. 2000, Proc. SPIE, 4008, 1010
Daddi, M., et al. 2001, A&A, 376, 825
Dale, D., & Helou, G. 2002, ApJ, 576, 159
Dale, D., et al. 2001, ApJ, 549, 215
Dannerbauer, H., Lehnert, M., Lutz, D., Tacconi, L., Bertoldi, F., Carilli, C., Genzel, R., & Menten, K. 2002, ApJ, 573, 473
Dannerbauer, H., et al. 2004, ApJ, 606, 664
Dunlop, J., et al. 2004, MNRAS, 350, 769
Dunne, L., Clements, D., & Eales, S. 2000, MNRAS, 319, 813
Dunne, L., et al. 2001, MNRAS, 327, 697
Eales, S., Bertoldi, F., Ivison, R., Carilli, C., Dunne, L., & Owen, F. 2003, MNRAS, 344, 169
Eales, S., Lilly, S., Webb, T., Dunne, L., Gear, W., Clements, D., & Yun, M. 2000, AJ, 120, 2244
Eales, S., et al. 1999, ApJ, 515, 518
Efstathiou, A., & Rowan-Robinson, M. 2003, MNRAS, 343, 322
Egami, E., et al. 2004, ApJS, 154, 130
Fixsen, D. J., Dwek, E., Mather, J. C., Bennett, C. L., & Shafer, R. A. 1998, ApJ, 508, 123
Flores, H., et al. 1999, ApJ, 517, 148
Franx, M., et al. 2003, ApJ, 587, L79
Frayer, D., et al. 1998, ApJ, 506, L7
———. 1999, ApJ, 514, 13L
———. 2003, AJ, 126, 73
———. 2004, ApJS, 154, 137
Garrett, M. 2002, A&A, 384, L19
Gear, W., et al. 2000, MNRAS, 316, 51L
Giavalisco, M., et al. 2004, ApJ, 600, L103
Glazebrook, K., et al. 2004, Nature, 430, 181
Greve, T., et al. 2004, MNRAS, 354, 779
———. 2005, MNRAS, in press
Haarsma, D., Partridge, R. B., Richards, E. A., & Windhorst, R. A. 2000, ApJ, 544, 641
Heckman, T. M. 2002, in ASP Conf. Ser. 254, Extragalactic Gas at Low Redshift, ed. J. S. Mulchaey & J. Stocke (San Francisco: ASP), 292
Helou, G., Soifer, T., Rowan-Robinson, M. 1985, ApJ, 298, L7
Holland, W. S., et al. 1999, MNRAS, 303, 659
Honda, M., et al. 2004, ApJ, 610, L49
Hughes, D. H., et al. 1998, Nature, 394, 241
———. 2002, MNRAS, 335, 871
Ivison, R. J., Smail, I., Le Borgne, J.-F., Blain, A. W., Kneib, J.-P., Bézecourt, J., Kerr, T. H., & Davies, J. K. 1998, MNRAS, 298, 583
Ivison et al. 2000, MNRAS, 315, 209
———. 2001, ApJ, 561, L45
———. 2002, MNRAS, 337, 1
———. 2005, MNRAS, submitted
Jenness, T., Lightfoot, J. F., & Holland, W. S. 1998, Proc. SPIE, 3357, 548
Kennicutt, R. C. 1998, ARA&A, 36, 189
Kneib, J.-P., et al. 2004, MNRAS, 349, 1211
Knudsen, K. K. 2004, Ph.D. thesis, Univ. Leiden
Komiyama, Y., et al. 2003, Proc. SPIE, 4841, 152
Kreysa, E., Gemund, H.-P., Raccanelli, A., Reichertz, L. A., & Siringo, G. 2002, in AIP Conf. Proc. 616, Experimental Cosmology at Millimeter Wavelengths, ed. M. De Petri & M. Gervasi (New York: AIP), 262
Ledlow, M., Smail, I., Owen, F., Keel, W., Ivison, R., & Morrison, G. 2002, ApJ, 577, L79
Lehnert, M., & Bremer, M. 2003, ApJ, 593, 630
Leitherer, C., et al. 1999, ApJS, 123, 3
Lewis, G., Chapman, S., & Helou, G. 2004, ApJ, in press
Lilly, S., et al. 1999, ApJ, 518, 641
Lu, Y., Cheng, K. S., & Zhang, S. N. 2003, ApJ, 590, 52
Lutz, D., et al. 1999, Ap&SS, 266, 85
———. 2001, A&A, 378, 70
Madau, P. 1995, ApJ, 441, 18
Madau, P., et al. 1996, MNRAS, 283, 1388
Magorrian, J., et al. 1998, AJ, 115, 2285
Martini, P., & Weinberg, D. 2001, ApJ, 547, 12
McCarthy, M., et al. 2001, ApJ, 597, 113
Meurer, G., et al. 1997, AJ, 114, 54
Muller, G., Reed, R., Armandroff, T., Boroson, T., & Jacoby, G. 1998, Proc. SPIE, 3355, 577
Neri, R., et al. 2003, ApJ, 597, 113
Neufeld, D. 1991, ApJ, 370, L85
Oke, J. B., et al. 1995, PASP, 107, 375
Omont, A., et al. 2001, A&A, 374, 371
———. 2003, A&A, 398, 857
Page, M., Stevens, J. A., Mittaz, J. P. D., & Carrera, F. J. 2001, Science, 294, 2516
Peacock, J., et al. 2000, MNRAS, 318, 535
Pettini, M., et al. 2001, ApJ, 554, 981
Reddy, N., & Steidel, C. 2004, ApJ, 603, L13
Richards, E. A. 2000, ApJ, 533, 611
Scott, S., et al. 2002, MNRAS, 331, 817
Serjeant, S., et al. 2003, MNRAS, 344, 887
Shapley, A., et al. 2003, ApJ, 588, 65
Shaver, P., et al. 1998, in ASP Conf. Ser. 156, Highly Redshifted Radio Lines, ed. C. Carilli, S. Radford, K. Menten, & G. Langston (San Francisco: ASP), 163
Silverman, J. D., et al. 2005, ApJ, 618, 123
Simcoe, R., et al. 2000, BAAS, 32, 758
Simpson, C., et al. 2004, MNRAS, 353, 179
Smail, I., Chapman, S., Blain, A., & Ivison, R. 2004, ApJ, 616, 71
Smail, I., Ivison, R., & Blain, A. 1997, ApJ, 490, L5
Smail, I., Ivison, R. J., Blain, A. W., & Kneib, J.-P. 2002, MNRAS, 331, 495
Smail, I., Ivison, R. J., Owen, F. N., Blain, A. W., & Kneib, J.-P. 2000, ApJ, 528, 612
Smail, I., et al. 1999, MNRAS, 308, 1061
———. 2003a, MNRAS, 342, 1185
———. 2003b, ApJ, 583, 551
Spoon, H., et al. 2004, A&A, 414, 873
Steidel, C., et al. 1999, ApJ, 519, 1
———. 2003, ApJ, 592, 728
———. 2004, ApJ, 604, 534
Stevens, J., et al. 2004, ApJ, 604, L17
Sturm, E., et al. 2000, A&A, 358, 481
———. 2002, A&A, 393, 821
Swinbank, M., Smail, I., Chapman, S., Blain, A., Ivison, R., & Keel, B. 2004, ApJ, submitted
Tacconi, L., et al. 2005, ApJ, submitted
Tran, Q. D., et al. 2001, ApJ, 552, 527
Tulloch, S. 2000, Newsl. Isaac Newton Group Telesc., 2, 26
van Dokkum, M., et al. 2003, ApJ, 587, L83
———. 2004, ApJ, 611, 703
Verma, A., Lutz, D., Sturm, E., Sternberg, A., Genzel, R., & Vacca, W. 2003, A&A, 403, 829
Wang, W., Cowie, L., & Barger, A. 2004, ApJ, 613, 655
Webb, T. M. A., Eales, S. A., Lilly, S. J., Clements, D. L., Dunne1, L., Gear, W. K., Flores, H., & Yun, M. 2003a, ApJ, 587, 41
Webb, T. M. A., et al. 2003b, ApJ, 582, 6
Wiklind, T. 2003, ApJ, 588, 736
Wolfe, A., et al. 2003a, ApJ, 593, 235
———. 2003b, ApJ, 593, 215
Yan, L., et al. 1999, ApJ, 519, 47L
Yun, M., & Carilli, C. 2002, ApJ, 568, 88
Yun, M., Reddy, N., & Condon, J. 2001, ApJ, 554, 803